Eberhard Karls University Tübingen
Faculty of Chemistry and Pharmacy
Interfaculty Institute for Biochemistry
Laboratory of Signal Transduction and Transgenic Models
Professor Doctor Robert Feil

Diploma Thesis in Biochemistry

Imaging of cGMP Signals in Vascular Smooth Muscle Cells

Submitted by:

Konstantinos Chatzieleftheriadis,

Department of Biochemistry & Biotechnology, University of Thessaly, Greece

Chatzieleftheriadis, Konstantinos:

Imaging of cGMP Signals in Vascular Smooth Muscle Cells

Diploma Thesis in Biochemistry

Eberhard Karls University Tübingen

Supervisor: Dr. Martin Thunemann, Interfaculty Institute for Biochemistry

April 2013 – August 2013, Tübingen

Table Of Contents

List of Abbreviations

ANP……atrial natriuretic peptide

APS……ammonium persulfate

BSA……..bovine serum albumin

CAG……chicken β-actin promoter with cytomegalovirus enhancer

cAMP……..cyclic adenosine monophosphate

CFP……cyan fluorescent protein

cGi500……..…cGMP indicator with EC_{50}≈500 nM

cGKI…..……..cGMP-dependent protein kinase I

cGMP……cyclic guanosine 3',5'-monophosphate

CLSM……..….confocal laser scanning microscopy

CNP……..c-type natriuretic peptide

DEA/NO……diethylamine NONOate

DMEM……Dulbecco's modified Eagle's medium

DNA…….....deoxyribonucleic acid

DTT……(*2S,3S*)-1,4-bis(sulfanyl)butane-2,3-diol

EGFP……enhanced green fluorescent protein

FBS……..fetal bovine serum

FRET……fluorescence resonance energy transfer

GC-A……..…….guanylyl cyclase A

GC-B……..…….guanylyl cyclase B

GFP……..green fluorescent protein

GTP……guanosine triphosphate

HEPES……..4-(2-hydroxyethyl)-1-piperazineethanesulfonic acid

HTNC……His-tagged, TAT-fusion Cre with nuclear localization signal

MARCKS……myristoylated alanine-rich c-kinase substrate

mcGi500……membrane-bound cGMP indicator with EC_{50}≈500 nM

MRP……multidrug resistance-associated protein

mT……membrane-targeted tdTomato

NO……nitric oxide

NOS……NO synthase

NP……natriuretic peptide

pGC……particulate guanylyl cyclase

PBS……phosphate buffered saline

PCR……polymerase chain reaction

PDE……phosphodiesterase

R26……ROSA26 locus

RNA……ribonucleic acid

ROI……region of interest

SDS……sodium dodecyl sulfate

SDS-PAGE……SDS polyacrylamide gel electrophoresis

sGC……soluble guanylyl cyclase

SMA……α-smooth muscle actin

SMC……smooth muscle cell

TCA……2,2,2-trichloroacetic acid

TEMED……tetramethylethylenediamine

UV……ultraviolet

VSMC……vascular smooth muscle cell

YFP……yellow fluorescent protein

Abstract

In the last decade, important progress has been made in the development of genetically encoded biosensors that can be used to detect and study second messengers like cyclic 3'-5' guanosine monophosphate (cGMP) in cells or living organisms. Recently generated transgenic mice that express cGi-type cGMP biosensors show a significant potential for research on this molecule and to study its spatiotemporal dynamics and a possible subcellular compartmentalization of its signaling pathways. In the current study, analysis of cGMP signals based on fluorescence resonance energy transfer (FRET), was performed in vascular smooth muscle cells (VSMCs) isolated from the murine aorta of transgenic, cGi-expressing mice. FRET cGMP biosensors located either in the cytosol (cGi500) or targeted to the plasma membrane (mcGi500) were tested and compared, upon application of special cGMP-elevating compounds like natriuretic peptides and the nitric oxide donor DEA/NO. VSMCs expressing either sensor, demonstrate different responses after exposure to cGMP-elevating agents that were applied either in constant or increasing concentrations. Responses showed different intensities, ranging from weak to strong cGMP transients. Importantly, differences were found between cGi500 and mcGi500 biosensors, in regard with responses induced after application of C-type natriuretic peptide, whereas only slight dissimilarities were observed after application of DEA/NO.

Περίληψη

Την τελευταία δεκαετία, έχει παρουσιασθεί σημαντική πρόοδος στην ανάπτυξη βιοαισθητήρων FRET εκφραζόμενων σε ζωντανούς οργανισμούς, ιστούς και κύτταρα με στόχο την ανίχνευση και τη μελέτη της κυκλικής 3'-5'-μονοφωσφορικής γουανοσίνης (cGMP). Διαγονιδιακά ποντίκια που εκφράζουν τέτοιους βιοαισθητήρες επιδεικνύουν ιδιαίτερη χρησιμότητα για τη μελέτη του μορίου αυτού, σε ό,τι αφορά τη χωρο-χρονική δυναμική και τον υποκυτταρικό εντοπισμό των σινιάλων του. Στην παρούσα μελέτη, έγινε παρακολούθηση των σημάτων cGMP σε αγγειακά λεία μυικά κύτταρα αορτής ποντικού έπειτα από χορήγηση ειδικών ενώσεων (ANP, CNP & DEA/NO), ενώ παράλληλα έγινε δοκιμή και σύγκριση μεταξύ βιοαισθητήρων FRET που εντοπίζονται κατά βάση στο κυτοσόλιο (cGi500) και στην κυτταροπλασματική μεμβράνη (mcGi500). Διαπιστώθηκε ότι τα αορτικά λεία μυικά κύτταρα παρουσιάζουν διαφορική συμπεριφορά ύστερα από εφαρμογή διαφόρων cGMP-επαγόμενων ουσιών, είτε σε ίδιες ή αυξανόμενες συγκεντρώσεις και πως οι προκαλούμενες αποκρίσεις αυτών μπορεί να παρουσιάζουν απών, ασθενή, ήπιο ή έντονο χαρακτήρα. Επιπλέον, βρέθηκαν διαφορές αναμεταξύ των δύο βιοαισθητήρων σχετικά με τη χορήγηση C-τύπου νατριουρητικού πεπτιδίου (CNP), αλλά μικρές μονάχα ανομοιότητες παρατηρήθηκαν αναφορικά με αποκρίσεις έπειτα από χορήγηση μορίου-δότη του μονοξειδίου του αζώτου (DEA/NO).

1 Introduction

1.1 Cyclic GMP

Cyclic guanosine 3′-5′ monophosphate (cGMP) is an important intracellular second messenger initially identified in rat urine in 1963 (Ashman, Lipton et al. 1963). It derives from guanosine-5'-triphosphate (GTP) which is an essential molecule for the synthesis of RNA and DNA. cGMP synthesis is induced by nitric oxide (NO) via NO-sensitive enzymes called soluble guanylyl cyclases (sGCs) which exist in two isoforms (sGC-1 and sGC-2) (Russwurm, Koesling 2002). Moreover, cGMP can also be produced by stimulation with peptide hormone factors called natriuretic peptides through the particulate guanylyl cyclases (pGCs), like GC-A and GC-B (Kuhn 2003).

After the synthesis of cGMP, its fate is the following according to existent knowledge so far: the cGMP-dependent serine-threonine kinases, cGKI and cGKII (also named PKG-I and -II) mediate most of the known cGMP effects (Hofmann, Feil et al. 2006); for instance, cGKI, which is highly expressed in smooth muscle cells, is involved in smooth muscle relaxation (Surks 2007). Apart from this kinase, there are additional cGMP effectors like the cGMP-regulated phosphodiesterases (PDEs); these enzymes catalyze the hydrolysis of the 3P-phosphodiester bond of cGMP or cAMP to yield GMP or AMP, respectively (Francis, Blount et al. 2011). Another target are the cyclic-nucleotide gated ion channels (CNG channels), a group of non-specific cation channels containing a carboxyl-terminal cyclic nucleotide-binding domain that is able to bind cAMP or cGMP (Biel and Michalakis 2009). Finally, it has been demonstrated that cGMP can exit the intracellular compartment and relocate into the extracellular space through the active efflux transporter MRP4 and MRP5 (Sassi, Lipskaia et al. 2008).

Experimental research has proved that cGMP and its descending effectors partake in many physiological and pathophysiological conditions. For example, it takes part in visual phototransduction, while it also contributes in the development of cardiovascular diseases, cancer and malaria which constitute the severest causes of death in modern human societies [(Chabre, Antonny et al. 1993); (Wolfertstetter et al. 2013)]. cGMP is also involved in the onset of milder but not less common pathologies like asthma (Placeres-Uray, Gonzalez de Alfonzo et al. 2010). Consequently, the choice of many researchers to interpret the biochemical effects of this molecule seems justified.

1.2 Natriuretic Peptides and pGC Receptors

The family of natriuretic peptides (NPs) consists of atrial natriuretic peptide (ANP), brain natriuretic peptide (BNP), C-type natriuretic peptide (CNP). Dendroaspis natriuretic peptide (DNP) and renal natriuretic peptide (urodilantin) are considered to belong to the same family as well. NPs are polypeptides of a relatively small length (22-53 amino acids) which demonstrate structural similarities, even though they are evolutionarily distinct (Inoue, Naruse et al. 2003).

ANP, BNP and CNP can regulate blood pressure and blood volume and are involved in modulating physiological processes such as fat metabolism, as well as pathophysiological phenomena like ventricular hypertrophy and pulmonary hypertension (Potter, Abbey-Hosch et al. 2006). ANP along with BNP are synthesized in atrial cardiomyocytes and secreted into circulation in response to cardiac wall stretch. Thus, they exert important cardiovascular functions by acting as endocrine factors. By contrast, CNP is mainly produced in vascular endothelial cells and chondrocytes, while it is also found in high concentrations in brain tissue [(Suga, Nakao et al. 1992); (Chusho, Tamura et al. 2001); (Sudoh, Minamino et al. 1990)]. It mediates the relaxation of vascular smooth muscle and inhibits the proliferation of VSMCs, a process that has been exploited to inhibit vascular pathogenesis [(Drewett, Fendly et al. 1995); (Furuya, Yoshida et al. 1991)]. CNP exhibits autocrine and paracrine regulatory functions in the cardiovascular system, as well as outside of it [(Sudoh, Minamino et al. 1990); (Suga, Nakao et al. 1992); (Hagiwara, Sakaguchi et al. 1994)].

Most of the known NPs are synthesized as pre-prohormones that undergo subsequent maturation, a process which leads to smaller forms containing a C-terminus of 17 amino acids which form a disulfide ring structure (Potter, Abbey-Hosch et al. 2006). The length of human preproANP is 151 amino acids and cleavage of the N-terminal signal sequence results in a precursor protein, proANP, of 126 amino acids. This molecule is the predominant form to be stored in granules. After secretion stimulus, the biologically active form emerges after a second cleavage step, catalyzed by the protease corin, as a 28 amino acid C-terminal fragment (Yan, Wu et al. 2000).

NPs are able to bind to three known transmembrane receptors: GC-A, GC-B, and the clearance (C) receptor (also known as NPR-C) that lacks guanylyl cyclase activity and participates in the metabolic clearance of the peptides (Fuller, Porter et al. 1988).

The main three members of NPs bind differentially to these receptors. GC-A is the receptor that mainly binds ANP and BNP, whereas GC-B represents the endogenous receptor for CNP [(Koller, Lowe et al. 1991); (Lopez, Garbers et al. 1997)]. In contrast, the clearance receptor binds all three ligands with similar affinity [(Bennett, Bennett et al. 1991); (Potter, Abbey-Hosch et al. 2006)].

GC-A and GC-B convert GTP into cGMP and pyrophosphate via their active catalytic domains. Thus, cGMP is the second messenger also in the signaling pathways of natriuretic peptides (Lucas, Pitari et al. 2000). The cGMP-generating receptors resemble growth factor receptor topology, containing an extracellular ligand-binding site (approximately 450 amino acids), a single hydrophobic membrane-spanning domain and an intracellular region of about 570 amino acids (Potter 2005). GC-A and GC-B receptors exist as homodimers, and they are inactive in the absence of ligand. Upon ligand binding, dimerization of the cyclase homology domain (CHD) follows, and this event is a prerequisite for the enhanced cyclase activity of these transmembrane receptors (Kuhn 2003).

GC-A mRNA is predominantly found in kidney, adrenal, vascular, pituitary and fat tissue. GC-B mRNA is observed also in above mentioned tissues and additional expression was reported, e.g. in chondrocytes [(Lucas, Pitari et al. 2000); (Potter, Abbey-Hosch et al. 2006)]. The clearance receptor is found to be localized to atrial, kidney and venous tissue, as well as to smooth muscle cells and endothelial cells of the aorta [(Fuller, Porter et al. 1988); (Porter, Arfsten et al. 1990); (Nagase, Katafuchi et al. 1997)].

1.3 Nitric Oxide and the sGC Receptor

NO is a significant signaling molecule produced by the enzyme NO synthase (NOS) from L-arginine and oxygen. In eukaryotic NO signaling, the initial event involves calcium increase, followed by binding of a calcium/calmodulin complex to NOS, which induces the activation of the enzyme. NOS enzyme exists in three isoforms: endothelial NOS (eNOS), neuronal NOS (nNOS), and inducible NOS (iNOS) [(Forstermann, Schmidt et al. 1991); (Alderton, Cooper et al. 2001)]. NO can diffuse freely across cell membranes alleviating the need for a transport system. Furthermore, it can exit a cell in which it is produced and enter neighboring cells. Outstanding example of this phenomenon is the diffusion of NO from endothelial cells to aortic VSMCs. Several chemical modifications have been linked to the actions

exerted by NO. For instance, S-nitration which is a post-translational modification involving the oxidative addition of NO to a thiol of proteins, induced by NO-derived reactive nitrogen oxide species (RNOS), such as peroxynitrite ($ONOO^-$) and nitrogen dioxide (NO_2) [(Eiserich, Hristova et al. 1998); (Schopfer, Baker et al. 2003); (Radi 2004)]. Additionally, a protein modification called S-guanylation occurs as well. This post-translational mechanism is based on the adduct formation of electrophilic 8-nitro-cGMP which is generated from NO, with sulfhydryl groups of cysteine (Sawa, Zaki et al. 2007). The meaning of this phenomenon *in vivo* is not yet fully elucidated. At a low, non-toxic concentration, the electronic structure of NO makes it also an excellent ligand for heme.

Thus, NO binds to sGC which is a histidine-ligated hemoprotein and is the only proven NO receptor (Derbyshire and Marletta 2012). sGC is heterodimeric in structure, and is composed of two subunits; α and β. As soon as NO binds to the heme of sGC, the enzyme is activated. The intracellular level of cGMP is therefore increased and signals are transmitted to its downstream targets. The $sGC/Fe^{+2}/NO$ complex and the second messenger cGMP contribute to many signal transduction events, most notably in the cardiovascular system (e.g. in the regulation of vascular tone and platelet function), as well as in the nervous system (e.g. in neurotransmission) (Derbyshire and Marletta 2012).

1.4 Regulation of the sGC, GC-A, and GC-B Receptors

In GC-A and GC-B receptors, there can exist three main states of receptor activity: basal, active, and desensitized (Potter, Abbey-Hosch et al. 2006). In the basal state the enzymatic activity is repressed. Upon ligand binding, a conformational change is induced, bringing together the juxtamembrane regions of the receptor extracellular domain (Labrecque, Mc Nicoll et al. 1999). This signal is thereafter transduced across the membrane and relieves the repression of the kinase homology domain (KHD) on the catalytic domain. Thus, the latter is allowed to dimerize, exposing two active sites on each dimer (Potter, Abbey-Hosch et al. 2006).

In their basal state and in the absence of ligands, GC-A and GC-B are highly phosphorylated, and prolonged exposure of receptors to NPs, induces reduction in receptor phosphate content that is correlated with reduction in NP-dependent stimulation of GC activity [(Potter and Garbers 1992); (Koller, Lipari et al. 1993); (Potter 1998); (Joubert, Labrecque et al. 2001)]. It is important to note, that ANP-dependent dephosphorylation results primarily from reduced phosphorylation, but not

from increased dephosphorylation (Joubert, Labrecque et al. 2001). Under basal conditions and as it was observed in mice, GC-A can be phosphorylated on four serines (S497, S502, S506, and S510) and two threonines (T500 and T513) within a 17 amino acid stretch at the amino-terminal portion of its KHD (Potter, Abbey-Hosch et al. 2006). Five of these sites (three serines and two threonines) were identified in human GC-A as well (Schroter, Zahedi et al. 2010, Yoder, Stone et al. 2010). The substitution of four or more phosphorylation sites to alanine, yields a receptor that is unresponsive to NPs, indicating that phosphorylation of GC-A is required for its activation by ANP and BNP (Potter and Hunter 1998). The less impaired glutamate-substituted version of GC-A though, has been reported to be resistant to ANP-dependent inactivation in membrane or whole cell preparations, which is an additional evidence that supports the desensitization by dephosphorylation model [(Potter and Hunter 1998); (Bryan and Potter 2002)].

GC-B has the same overall topology as the GC-A receptor. GC-B can be phosphorylated on two threonines (T513, T516) and four serines (S518, S523, S487 and S526). These phosphorylation sites were identified in rat and human GC-B [(Potter and Hunter 1998); (Yoder, Stone et al. 2010)]. Similarly to GC-A, mutating any of these amino acids to alanine or glutamate, reduces NP-dependent GC activity (Yoder, Stone et al. 2010).

Apart from NPs, there are also other molecules that regulate the activity of these receptors. For instance, protein kinase C (PKC) activators are found to be involved in the dephosphorylation and desensitization of GC-B, but in a different fashion than the NP-dependent dephosphorylation (Potter and Hunter 2000). Furthermore, agents or conditions that elevate intracellular calcium concentrations can cause reduced phosphorylation of GC-B [(Potthast, Abbey-Hosch et al. 2004); (Abbey-Hosch, Smirnov et al. 2005)]. On the other hand, ATP has been found to positively regulate the GC-A and GC-B receptors *in vitro* [(Foster and Garbers 1998); (Abbey-Hosch, Smirnov et al. 2005)].

Apart from the mechanisms mentioned above, there are also other regulating events associated with the control of the abundance of receptors at the cell surface. Receptor degradation or receptor internalization after ligand binding is a characteristic example (Flora and Potter 2010). Other mechanisms that influence receptor activity are the control of local ligand availability by sequestrating NPs via the clearance receptor or by ligand degradation through the insulin-degrading enzyme [(Matsukawa, Grzesik et al. 1999); (Ralat, Guo et al. 2011)].

As far as NO and sGC are concerned, maximal sGC activation gradually decreases after repetitive NO exposure, and this process refers to the desensitization of sGC (Bellamy, Wood et al. 2000). There is evidence which supports that S-nitrosylation contributes to sGC desensitization [(Sayed, Baskaran et al. 2007); (Sayed, Kim et al. 2008)]. There are two different sGC/NO states which occur *in vitro* after NO binding, and there exist two models: the model of the dissociation of NO and the deactivation of NO-stimulated sGC (Derbyshire and Marletta 2012). NO dissociation from the heme of sGC is slow, whereas the deactivation of sGC/Fe^{+2}/NO complex is rapid, considering *in vitro* measurements. Therefore, NO-dependent deactivated sGC enzymes differ from unligated sGC species derived from the dissociation of NO from the heme and it has been suggested that two molecules of NO are able to bind to sGC. The importance of the two different sGC/NO states and the mechanism of sGC activation *in vivo* remain elusive.

1.5 Aorta and cardiovascular system

1.5.1 Anatomy and main function of the aorta

The aorta constitutes the main blood vessel of the body and is divided into three anatomical parts: the ascending, the descending, and the abdominal aorta (De Graaf, 1998; Tortora 1994). The ascending aorta begins at the left ventricle of the heart and rises up in the front of the chest towards the top of the body. At that level, it takes a hairpin turn which is called “aortic arch”, towards the back of the body. From the aortic arch, the descending aorta progresses at the spine down to the chest, through the thoracic diaphragm into the abdomen. Opposite the lower border of the fourth lumbar vertebra, the abdominal aorta is separated into two blood vessels, the common iliac arteries and a smaller vessel, the median sacral artery (Putz, Pabst 2006).

The aorta distributes oxygenated blood to all parts of the body (Waschke 2011). The ascending aorta supplies the coronary arteries which provide blood to the heart itself. The aortic arch emits all important branches to the head, brain, and arms. The descending aorta sends branches to each costal. The abdominal aorta gives off branches to liver, intestines, kidneys, and other important internal organs. Finally, each of the terminal branches of the abdominal aorta goes to one of the legs.

Like all arteries, the aortic wall is composed of three layers: the intima, the media, and the adventitia. The intima is the innermost layer which constitutes a single layer of endothelial cells which align according to the flow, resting on a sub-endothelial layer of elastin and collagen which anchors to the internal elastic lamina (Rhodin 1979). The internal elastic lamina is a membrane that separates the intima from the media and consists of collagen type IV, fibronectin, and laminin. It acts as a cushion that allows bending and changes in diameter associated with changes in blood pressure (Silver et al. 1989). The media is the middle layer which consists of smooth muscle and elastic fibers. This structure allows the aorta to contract and relax through a complete cardiac cycle. Finally, the adventitia which is the outer layer, provides additional support and structure to the aorta.

1.5.2 Human and mouse aorta

The hemodynamics of human and mouse aorta has been compared and contrasted by many researchers in recent years to investigate whether it is indeed purposeful to study the mouse as a model for vascular physiology and diseases in human (Suo, Ferrara et al. 2007, Trachet, Swillens et al. 2009, Casteleyn, Trachet et al. 2010).

Evidence demonstrates that the topography of the murine and human hearts and the branching patterns of their aortic arches present many analogies (Casteleyn, Trachet et al. 2010). For instance, both in mice and humans, the initial segment of the aorta is sigmoidally curved. Moreover, a non-planar geometry of the aortic arch is present in both species. The aortic arches of mice and older men seem anyhow, to share most similarities. The ascending and descending aorta of mice are not positioned in a single vertical plane (non-planar aortic geometry). This characteristic configuration is also present in humans, albeit least pronounced in younger men. However in mice, the transition between both aortic segments is more fluent and the aortic arch is positioned more transversely in the thorax (Casteleyn, Trachet et al. 2010).

1.6 Vascular Smooth Muscle Cells (VSMCs) from the aorta

1.6.1 General characteristics

Vascular smooth muscle contracts or relaxes to change the volume of blood vessels, as well as the local blood pressure, a mechanism that is responsible for the redistribution of blood within the body to areas where it is needed, such as areas with temporarily enhanced oxygen consumption. Smooth muscle relaxation has been found to be induced via the NO/cGMP signaling pathway and one major effector implicated in this procedure, is the cGKIα isoform (Feil, Gappa et. al 2002).

VSMCs contribute to the structural integrity of the blood vessels and their primary function is to regulate the diameter of the blood vessels in response to physiological stimuli (Metz, Patterson et al. 2012). Pathologically, excessive vasoconstriction results in hypertension, while excessive vasodilation results in hypotension.

It has been established that VSMC phenotype is characterized by a dynamic nature and heterogeneity *in vivo* (Rensen, Doevendans et al. 2007). These phenotypes have been termed “contractile” and “synthetic” (figure 1.1), based on their primary functions of contraction or synthesis of extracellular matrix (ECM) proteins, respectively (Miano 2003). The contractile state is what is considered to be the primary state of VSMCs in a healthy aorta, while synthetic phenotypes have been observed *in vivo* during development, in response to injury followed by tissue repair, and in inflammatory response within the microenvironment of an atherosclerotic lesion (Louis and Zahradka 2010).

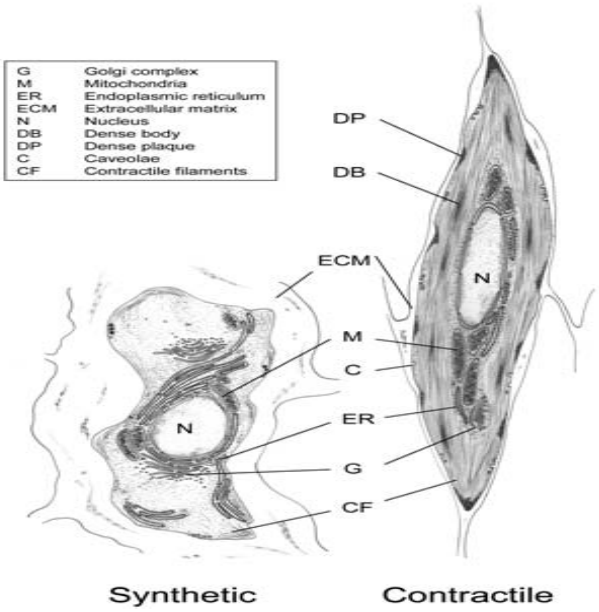

Figure 1.1. Characteristics of VSMCs in the synthetic and contractile phenotypic state. Adopted from Rensen, S. S., et al. (2007) "Regulation and characteristics of vascular smooth muscle cell phenotypic diversity." Neth Heart J **15**(3): 100-108.

1.6.2 Role of VSMCs in the onset of atherosclerosis

Atherosclerosis literally stands for the thickening of an artery wall and this is a progressive process responsible for most heart diseases. This disease state is considered as the leading cause of death for advanced-aged adults in most developed countries (Weber and Noels 2011). Different cell types partake in the onset of this condition, such as macrophages, white blood cells, monocytes, endothelial cells, and platelets [(Ross 1999); (Galkina and Ley 2009)]. It has been found that aortic VSMCs contribute to this complex and time-requiring condition as well: Calcification, apoptosis, proliferation and migration from the media to intima are key events which play important roles in its pathogenesis (Rudijanto 2007).

Interestingly, cyclic GMP has been found to be implicated in all those crucial events [(Kanno, Into et al. 2008); (Sarkar, Meinberg et al. 1996); (von der Leyen, Gibbons et al. 1995); (Pollman, Yamada et al. 1996)]. However, there are contradictory results in the literature regarding some aspects, such as proliferation [(Boerth, Dey et al. 1997), (Hassid, Arabshahi et al. 1994)]. This fact implies the possibility that VSMCs may respond differently to the same stimuli or that there are regulatory mechanisms that are not yet fully understood or remain to be identified.

1.7 Transgenic mice and the Cre/*lox* recombination system

Transgenic animals are extensively used in research to study *in vivo* gene function in respect with development and pathogenesis. It is achievable to evaluate therapeutic approaches in models of human disease and to investigate progression of diseases in a manner which is hardly feasible to study in human patients.

A transgenic animal can be generated by several methods which include microinjection of a DNA fragment into the pro-nucleus, embryonic stem cell manipulation and injection, sperm-mediated transgenesis, and viral infection of pre-implanted embryos (Tian, Wang 2007). The microinjection method is one of the most widely used approaches so far.

The mouse (Mus musculus) is one of the most utilized organisms for research. Transgenesis in mice is a widely used approach to generate models of human disease. Transgenic mice offer the advantages of relatively low cost and a short gestation time which ranges from 18.5 to 21 days (Gama Sosa, De Gasperi et al. 2010). Additional advantages are the availability of genetically inbred strains and the relatively close evolutionary relationship of mice and humans. Moreover, a variety of technologies for introducing genetic modifications within specific loci (e.g. the ROSA26 locus), into the mouse genome is also available [(Gama Sosa, De Gasperi et al. 2010); (Casola 2010)]. Genetic modifications including deletions, mutations, inversions or translocations can be introduced using the gene targeting technology.

One technology that permits inducible gene expression in specific tissues is the Cre/*lox* recombination system (Novak, Guo et al. 2000). Cre recombinase is a type I topoisomerase from P1 bacteriophage that catalyzes abscission and site-specific recombination of DNA sequences between *loxP* sites (Hamilton and Abremski 1984). Recombination products are dependent on the location and relative orientation of the *loxP* sites: Two DNA segments containing single *loxP* sites will be fused, whilst DNA between such sites in the same orientation will be excised in circular form. Lastly, DNA between opposing *loxP* sites will be inverted with respect to the rest of the DNA. The reactions of recombination proceed via covalent recombinase-DNA intermediates with conservation of phosphodiester bond energy, and requires no DNA synthesis (Feil 2007).

To introduce transgenes with *loxP* sites in the mouse genome, the technology of homologous recombination in ES cells is utilized [(Copeland, Jenkins et al. 2001); (Court, Sawitzke et al. 2002)]. The targeting construct is designed to have two *loxP* sites flanking one or more exons of the gene of interest and positioned in the

surrounding introns, so that they do not intervene with gene expression. In the construct, it is also included a *loxP* flanked stop cassette, to block ubiquitous transgene expression and to allow its expression only upon introduction of Cre recombinase. The mice which carry in their genome the *loxP* flanked version of the target gene are then crossed to mice selectively expressing Cre recombinase in specific tissues, generating descendants with permanent inactivation or activation of the respective gene based on the pattern of Cre expression. This pattern can be controlled by cell type-specific promoters. The Cre/*lox* system is the most useful and efficient tool for site-specific genome engineering in the mouse.

Gene knock-in strategies have been used to replace or mutate genes at a particular locus in a chromosome (Nilles and London 2007). The gene of interest can be labeled to clarify its expression pattern with a reporter gene such as GFP. In knock-in mice, reporters are expressed at the same time (age) and with the same tissue distribution as the native gene and are ideal for localizing gene expression. Importantly, replacement of a indigenous gene (e.g. prkg1) with a transgene by this targeting method has been used in the generation of cGMP FRET sensor knock-in mice (Thunemann, Wen et. al 2013).

1.8 Biosensors of cGMP and FRET as a tool for studying living cell biochemistry

The design of genetically encoded fluorescent biosensors for cGMP is a major technical achievement, as it allows real-time monitoring of cGMP signals in various types of living cells (Thunemann, Fomin et al. 2013). These biosensors are composed of variants of the green fluorescent protein (GFP), such as the yellow (YFP) and the cyan (CFP) fluorescent protein. Most of the recently designed sensor proteins detect cGMP by the principle of FRET. This biophysical phenomenon is based on the transfer of energy from an excited donor fluorophore (e.g. CFP) to an acceptor fluorophore (e.g. YFP) in a non-radiating fashion via long-range dipole-dipole interactions (Förster, 1946). The donor and acceptor fluorophores must be in close proximity (2-6 nm) and in appropriate orientation in respect to each other. Furthermore, the donor's emission spectrum must overlap with the acceptor's excitation spectrum (Zaccolo 2004). Most FRET-based cGMP sensors consist of one or two cGMP-binding domains derived either from PDEs or from cGKs. Those elements are positioned between the fluorophores (CFP and YFP). Upon cGMP binding, a conformational change occurs to the structure of the sensor causing a

change in the distance and/or orientation of the fluorophores to each other. Thereby, cGMP binding can induce either an increase or a decrease of the FRET efficiency, depending on the type of sensor (Thunemann, Fomin et al. 2013). A change in FRET efficiency is depicted by calculating either the ratio of YFP over CFP emission or *vice versa*. In a cell expressing the sensor, the change of the CFP/YFP (or YFP/CFP) ratio therefore reflects the change of cGMP levels within the cell.

The FRET-based cGi-type (for “cGMP indicator”) sensors designed by Russwurm and colleagues, are useful tools for cGMP imaging in intact cells and tissues of organisms [(Norris, Ratzan et. al 2009); (Thunemann, Wen et. al 2013); (Couto, Oda et. al 2013)]. Here, binding of cGMP to the binding site of this cGKI-based biosensor induces a decrease of the FRET efficiency (Russwurm, Mullershausen et al. 2007). The FRET changes in cGi sensors are usually presented as donor-acceptor emission ratio (CFP/YFP), so that an increase in the cGMP concentration is illustrated by an increase in the emission ratio. The cGi-type sensors fulfill successfully the criteria of speed, amplitude, and reversibility of the FRET change as well as high sensitivity and selectivity to cGMP over cAMP (Russwurm, Mullershausen et al. 2007).

Cyclic GMP can also be detected through another category of sensors, which is not FRET-based. Outstanding paradigm of this category is FlincG (for “fluorescent indicator of cGMP”). FlincGs are composed of a single circularly permutated EGFP (cpEGFP) fused to the regulatory domain of cGKI containing two cGMP-binding domains. Here, cGMP binding causes a detectable increase in GFP fluorescence intensity (Nausch, Ledoux et al. 2008).

1.9 Goals

Research on transgenic mice expressing the cytosolic cGi500 biosensor has been successfully performed and published (Thunemann, Wen et. al 2013). However, major research in relation with transgenic mice expressing the membrane-bound mcGi500 biosensor has not been done nor published.

In this study, mcGi500 biosensor expressed in VSMCs isolated from R26-CAG-mcGi500 mice was tested and utilized in direct comparison with cGi500 VSMCs isolated from R26-CAG-cGi500 mice (mixed culture). Basic aims of the study, were the characterization of the cell cultures by immunocytochemistry, as well as the verification of different localization between cGi500 and mcGi500. An important aspect of the current study was the investigation of possible differences between the

two FRET sensors in detecting cGMP spatiotemporal signals in response to cGMP-modulating agents (e.g. CNP and DEA/NO). Furthermore, it was a matter of interest to study if there was diversity or homogeneity in responses associated with the exerted cGMP signals within the VSMCs from the aorta. Finally, it was under the scope of examination whether the R26-CAG-mT/mcGi500 allele could be converted to R26-CAG-mcGi500 *in vitro*, in SMCs and if the recombined SMCs could be monitored afterwards via FRET microscopy, in regard with cGMP responses.

2 Materials and Methods

Transgenic Mice (R26-CAG-cGi500 and R26-CAG-mcGi500)

R26-CAG-cGi500 or R26-CAG-mcGi500 transgenic mice (species: Mus musculus; strain: 129Sv/C57BL6N) resided in a conventional mouse facility at 22^{o}C and 50-60% humidity in a 12h/12h light/dark cycle with free access to standard rodent chow and tap water. Both male and female mice were used for experiments. Animal procedures were performed with supervision and were approved by the Regierungspräsidium Tübingen.

2.1 Materials

2.1.1 Reagents, Media, Solutions and Drug Substances

Solutions for PCR-based Genotyping

Proteinase K reaction mix
prepare freshly

Proteinase K (50 µg/µL, Roth) 1 µg/µL 1 µL

10x Reaction Buffer S (Peqlab) 1x 5 µL

H_2O (milliQ) 44 µL

1×TBE
adjust pH to 8.3, store at room temperature

0.5 M Tris (Roth) 10.8 g

0.5 mM H_3BO_3 (Roth) 5.5 g

10 mM EDTA (Roth) 4 mL

H_2O (milliQ) 996 mL

6×DNA loading dye
store at 4°C

40% Sucrose (Roth) 2 g

0.125% Bromophenol blue (Roth) 6 mg

0.125% Xylene cyanol (Roth) 6 mg

1×TBE add 5 mL

Solutions for Cell Culture

Culture medium with 10% FBS
store at 4°C

DMEM with GlutaMAX (Invitrogen)

FBS (Invitrogen, heat-inactivated) 10%, stored at -20°C

100×Pen/Strep (Invitrogen) Penicillin: 10000 U/mL; Streptomycin: 100 µg/mL

Serum-free culture medium
store at 4°C for up to 2 months

DMEM with GlutaMAX (Invitrogen)

100×Pen/Strep (10000 U/mL / 100 µg/mL, Invitrogen) 100 U/ml / 1 µg/mL

Phosphate-buffered saline (PBS) (Ca^{2+}/Mg^{2+} free, pH 7.4)
adjust pH to 7.4 with HCl or NaOH, aliquot, autoclave and store at room temperature

135 mM NaCl 7.89 g/L

3 mM KCl 0.22 g/L

8 mM $Na_2HPO_4 \cdot 2\ H_2O$ 1.42 g/L

2 mM KH_2PO_4 0.27 g/L

H_2O (double-distilled)

1×Trypsin/EDTA
store at 4°C

10×Trypsin/EDTA (Invitrogen) Trypsin: 5 g/L , EDTA: 2 g/L

PBS

HTNC-Cre
adjust pH to 7.4, store at -20°C
440 µM HTNC-Cre in:
50% Glycerol (Roth),
1 M NaCl (Roth) and
20 mM HEPES (Roth)

All the solutions for cell culture besides HTNC-Cre were preheated to 37°C before use. Sterile conditions within the cell culture hood, were guaranteed by using 70% ethanol and UV radiation. Washing the bench with 70% ethanol is required before and during work under the cell culture hood in order to keep a contaminant-free environment. Pipettes with contents destined for cell culture were used only under sterile conditions (cell culture hood).

Tools and solutions for FRET

Inverted microscope (Axiovert 200 with 1.0/1.6x Optovar lens, Carl Zeiss).

Fluorescence-grade objectives with 10x and 40x magnification (Plan NeoFluar 10x/0.30; EC Plan NeoFluar 40x/1.30 Oil, Carl Zeiss).

Computer-controlled light source (Oligochrome, TILL Photonics).

FRET filter set: 445/20 nm CFP excitation filter and 470 nm dichroic mirror (AHF or Chroma Technology).

Beam splitter (Micro-Imager DUAL-View, Photometrics) with 05-EM insert (516 nm dichroic mirror, 480/50 nm CFP and 535/40 nm YFP emission filters) placed between microscope and camera.

Series 20 Chamber (Warner Instruments).

Single Channel Heater Controller (TC-324B, Warner Instruments).

SF-28 Sloflo In-line Solution Heater (Warner Instruments).

YFP filter set: 497/16 nm excitation filter, 516 nm dichroic mirror, 535/22 nm emission filter (AHF or Chroma Technology).

Cooled electron-multiplying charged-coupled device (EM-CCD) camera (Retiga 2000R, QImaging).

Superfusion system: FPLC pump (Pharmacia P-500, GE Healthcare), FPLC injection valves (Pharmacia V-7, GE Healthcare), superfusion chamber (Warner Instruments), vacuum pump with adjustable vacuum, sample loops (e.g. 2, 5, 20 mL), tubing, connectors, hypodermic needles, and syringes.

Image acquisition and online analysis software (Live Acquisition, TILL Photonics), image analysis software for offline analysis (Offline Analysis, TILL Photonics; ImageJ), data analysis software (Microsoft Excel, Microsoft; Origin, OriginLab Corp.).

20% denatured ethanol.

100 mM DEA/NO
aliquots (50 µL), store at −20°C
Dissolve 50 mg DEA/NO in 2.42 mL ice-cold 10 mM NaOH.

100 mM ANP
aliquot (50 µL), store at −20°C
Dissolve 0.1 mg ANP (1-28, rat) in 0.327 mL ddH_2O.

100 mM CNP
aliquot (50 µL), store at −20°C
Dissolve 0.5 mg CNP (1-22, rat) in 2.275 mL ddH_2O.

Tyrode buffer
adjust pH to 7.4, aliquot, autoclave, and store at room temperature
140 mM NaCl (Roth) 8.18 g/L
5 mM KCl (Roth) 0.373 g/L
1.2 mM $MgCl_2$ (Roth) 0.244 g/L
2 mM $CaCl_2$ (Roth) 0.9 g/L
5 mM HEPES (Roth) 2.38 g/L
H_2O (milliQ)

Solutions for Immunostaining

PBS-Formaldehyde 3.7%
prepare freshly, chill on ice

37% Formaldehyde (Roth) 1.5 mL

PBS add 15 mL

0.5% BSA-PBS
prepare freshly

BSA (Roth) 5 g/L

PBS

Serum-PBS
prepare freshly

5% Normal Goat Serum (Vector Laboratories) 0.5 mL

BSA-PBS add 10 mL

Hoechst 33258
store in -20°C

Hoechst 33258 (Sigma) 1µg/µL

20% Triton-X 100
store at room temperature

Triton-X 100 (Roth) 20 mL

H_2O (double-distilled) add 80 mL

80 % Glycerol
microwave until dissolved, autoclave, store at room temperature

Glycerol (Roth) 60 mL

H_2O (double-distilled) add 15 mL

Solutions for subcellular fractionation

Subcellular fractionation buffer:

250 mM Sucrose (Roth)

20 mM HEPES (Roth) (pH 7.4)

10 mM KCl (Roth)

1.5 mM $MgCl_2$ (Roth)

1 mM EDTA (Roth)

1 mM EGTA (Roth)

The following are to be used at the time of use:

1 mM DTT (Roth)
100 mM PMSF (Roth)

Protein Precipitation

TCA
store at room temperature

100% (w/v) trichloroacetic acid (TCA) (Roth)

Dissolve 5 g TCA into 3.5 mL H_2O (milliQ).

Solutions for SDS-PAGE

4× Resolving gel buffer
adjust pH to 8.8, store at 4 ^oC

1.5 M Tris (Roth) 182 g/L

0.4% SDS (Roth) 4 g/L

H_2O (milliQ)

4× Stacking gel buffer
adjust pH to 6.8, store at 4 ^oC

0.5 M Tris (Roth) 60.4 g/L

0.4% SDS (Roth) 4 g/L

H_2O (milliQ)

20% APS
aliquot, store at -20 ^oC, avoid long exposure to light

20% APS (Roth) 2 g

H_2O (milliQ) add 10 mL

10× SDS running buffer
do not adjust pH, store at room temperature, prepare working solution as 1:10 dilution, freshly

0.25 M Tris (Roth) 30.2 g/L

2 M Glycine (Roth) 144 g/L

1% SDS (Roth) 10 g/L

H_2O (milliQ)

2.2 Methods

2.2.1 Polymerase Chain Reaction (PCR)

The polymerase chain reaction (PCR) is a highly sensitive method to amplify enzymatically defined DNA sequences *in vitro* (Saiki, Gelfand et al. 1988). In a cyclic process, the two strands of the DNA double helix are physically separated first by high temperature (95^{o}C). After this initial step, and at lower temperatures, template-specific oligonucleotide primers hybridize (50-65^{o}C). Then, at optimal working temperature (e.g. 72^{o}C), a thermostable DNA polymerase such as Taq polymerase, elongates the primers in 5'-3' direction. By repeating DNA melting, primer hybridization and DNA polymerization, the template DNA defined by the binding site of two primers, is amplified in an exponential fashion.

PCR was used to determine the genotype of transgenic mice used for aortic VSMC preparation as described before (Feil, Valtcheva et al. 2009). DNA was isolated from the ear patch area of mice. Tissue was incubated with digestion mix (50 µL for each sample) in the oven (55^{o}C) overnight, along with proteinase K which is a broad-spectrum serine protease. The used primer pairs have been mentioned and given in detail in published work (Thunemann, Wen et. al 2013).

2.2.2 Tissue Isolation

VSMCs from the aorta, BSMCs and CSMCs were isolated from mice as previously described (Thunemann, Fomin et al. 2013). Transgenic mice that ubiquitously expressed cGi500 or mcGi500 biosensor, were sacrificed and used for tissue isolation. For VSMC preparation, four aortae had to be isolated for each sensor in order to acquire sufficient amount of VSMCs to be seeded in 24-well plates. The age of mice ranged from 1 to 4 months.

Mice were sacrificed by inhalation of carbon dioxide. Using ice-cold PBS and working on ice are necessary procedures while working after the isolation of smooth muscle-rich tissues. The main reason for this is that the degradation should be as low as possible in a period of time. For VSMCs, surrounding fat and connective tissue were removed from the aorta. Then, tissues were cut into 5-mm pieces and incubated at 37^{o}C for 45 minutes with papain (0.7 mg/mL), followed by 10-15 minutes with collagenase (1 mg/mL) and hyaluronidase (1 mg/mL); tissues were dissociated by pipetting through a 1000-µL pipette tip. The amount of wells and culture plates

was chosen according to the availability of viable cells, counted by trypan blue exclusion. Thereinafter, cells were suspended in culture medium (DMEM with 4.5 g/L glucose, 100 U/mL Penicillin, 100 µg/mL Streptomycin, 10% FBS) in 24-well plates and they were grown in an incubator (CO-170, Innova) at 37°C and in humidified atmosphere (94% air, 6% CO_2), until the time of use.

2.2.3 Cell culture

2.2.3.1 Medium change

Three days after the isolation of primary VSMCs, the cells in the 24-well plates were washed once or twice with 0.4 mL of PBS and afterwards 1 mL of fresh pre-warmed medium was added to each well. In a period of 3-4 days, the medium was changed and replaced by fresh one. 24 hours prior of FRET measurements or immunostaining, the medium was changed into serum-free as growth factors contained in the serum might interfere with cGMP signaling and with the phenotype of VSMCs.

2.2.3.2 Passaging of VSMCs from the aorta

VSMCs grown up to 90% of confluency were allowed to be passaged. Normally, the faster the cells grew the higher the ratio used for passaging. The ratios were in the range of 1:2 to 1:6. Passaged cells were distributed between wells using the same ratio. Cells should be passaged when they reach 70 to 90% confluency. Do not allow the cells to acquire 100% confluency as the capacity for exponential growth may be diminished.

1. Aspirate medium from the cell culture well.
2. Wash cells once by adding 100 µL/cm^2 of pre-warmed (approx. 37°C) PBS, then aspirate PBS.
3. Add 50 µL / cm^2 of detachment enzyme (Trypsin / EDTA) to the wells.
4. Incubate at 37°C until cells are rounded and start to detach. Check for cell detachment under the microscope.
5. Tap carefully the culture well plate.
6. Rinse the bottom of the culture well 2 to 3 times with the suspension to remove all cells and to separate them into a single cell suspension.

7. Stop the enzymatic reaction by adding 3x volume the amount of fresh pre-warmed medium.
8. Transfer cell suspension into a falcon tube.
9. Centrifuge cells for 10 minutes, 1200 rpm at room temperature (Centrifuge 5804 R, Eppendorf).
10. Aspirate supernatant and resuspend the pellet in 1 to 2 mL medium.
11. Seed viable cells with 4 x 10^3 / cm^2.

2.2.4 Fluorescence Resonance Energy Transfer (FRET)

The fluorescence resonance energy transfer (FRET) between two molecules (donor and acceptor) is a biophysical phenomenon first described by Förster in 1946. Today, it is mainly used in understanding various intracellular signaling entities as a part of biochemical research, as well as in drug discovery. In the process of FRET, initially a donor fluorophore absorbs the energy due to the excitation of incident light and transfer the excitation energy to a nearby chromophore, the acceptor.

In this study, FRET was used to monitor cGMP in real-time, in living transgenic VSMCs, after applying specific substances. Cells were grown at 37^{o}C and 6% CO_2, in cell culture medium (DMEM with 10% FBS) for 4 up to 14 days until FRET analysis.

The followed protocol is the below:

1. Select wells with cells having the appropriate morphology and confluency and place them in serum-free medium at least 24 hours prior any measurements.
   FBS that is present in serum contains constituents such as a variety of growth factors which some of them (e.g. fibroblast growth factor) could interfere with the cGMP signaling pathway and with the smooth muscle phenotype.
2. Before starting measurements, set the light source on power at least 30 minutes prior and rinse the superfusion system with 20% denatured ethanol for 10 minutes. After this washing step, rinse with the Tyrode Buffer solution for 10 minutes.
3. Degas the Tyrode with ultrasound for 5 minutes (Elma S 30 H).
4. Open the computer application software (Live Acquisition software, TILL Photonics) and fix the camera alignment via a special microscopic slide (Photometrics).

5. Put silicon (GE Bayer) on the chamber (Warner Instruments), only close to the borders and wipe off the excess of it with a cotton bud.
6. Transfer coverslip via a forceps and a needle (21 gauge), with the cells facing upside, into a tissue culture petri dish (35 x 10 mm, Cellstar) filled with 1.5 mL of pre-warmed Tyrode.
7. Mount coverslip to the bottom of the small chamber (Series 20, Warner Instruments), with the cells facing to the inside of the chamber.
8. Put firmly together the chamber with the magnets and then immediately add 500 μL of Tyrode Buffer onto the coverslip to ensure cell vitality.
9. To measure with 40x, select the appropriate lens and place on its top, a drop of oil (Immersol 518 F, Zeiss).
10. Remove liquid from the lower part of the coverslip with a tissue paper (11 x 21 cm, KimTech Science), so that any humidity would not mix with the oil drop.
11. Transfer the chamber carefully into the stage and plug the cables that belong to the superfusion system and the FPLC pump.
12. Allow flow of Tyrode (at 60 mL/h*)* into the chamber and be cautious for any possible leakage. Do not continue the experiment, until you establish a stabilized, constant flow by adjusting the vacuum and the level of the outlet needle.
13. Attach carefully the lens to the middle of the coverslip.
14. Excite coverslip with cells, with the appropriate wavelength in the respective filter (e.g. for YFP, 497/16 nm, 516 nm dichroic mirror) and look for an area with the favorable cells.

    Use half or below of the light power of the channel to avoid photo-oxidative stress as much as possible.
15. Arrange the appropriate acquisition program settings: Binning, Cycle, Exposure Time etc. according to the needs of the experiment.
16. Illustrate field of view from the microscope to the computer screen.
17. Draw ROIs (Regions Of Interest), so that cells are marked and will be analyzed during the FRET measurement.
18. Change to CFP filter (445/20 nm, 470 nm dichroic mirror) and start the measurement in the dark.

    Leave a slight light source on, so that you can perform accurately while you are doing the experiment.
19. Change to lower levels of the parameters “Exposure Time” and “Cycle”, only if a noticeable change in the distribution of the biosensor (appearance of bright spots) is observed.

This is an indication of photo-bleaching effect which might critically interfere with the monitoring of the cell responses. Therefore in that case, new ROIs from another field of view must be obtained.

20. Allow at least 60 frames (1 frame=5 s) to obtain a baseline which is necessary for further evaluation of the experiment.
21. Dilute the drug of interest into a falcon tube with 3 mL of the same Tyrode in a particular concentration.
    Note that for preparation of DEA/NO, a special manipulation is needed (see below).
22. After addition of the drug into the 2 mL-injection loop, turn manually from "Load" to "Inject", and wait until a response (change between the CFP/YFP ratio) which would be represented normally as a formation of a curve.
    That indicates that cells do respond to the stimulus.
23. Wait for the curve to return as close to the baseline, before any next drug application.
    Between the application of two different drugs, the injection loop is rinsed automatically with Tyrode.
24. Repeat steps 21-23, according to the goals of each experiment.
25. At the end of the experiment, disassemble carefully the chamber and use ddH_2O onto tissue paper to clean the silicon grease.
26. Rinse the superfusion system with 20% denatured ethanol at the end of series of experiments.

The following drugs were used: ANP, CNP, DEA/NO, and stocks were kept on ice during measurements. ANP and CNP were diluted in 3 mL of Tyrode and used immediately. 1 μL of DEA/NO was diluted in a falcon tube with 1 mL of 10 mM NaOH and then from this solution the final dilution with the favorable concentration was achieved into another falcon tube containing 3 mL of Tyrode, according to the needs of each experiment. Note that the half-life of DEA/NO is approximately 12-15 minutes at 37^{o}C, so a fresh drug dilution after this period of time is necessary.

2.2.5 Evaluation of the data

The evaluation of the FRET measurements is a crucial procedure, as it provides us with an amount of valuable information associated with the behavior of each cell to a specific stimulus that may exert cGMP production. Moreover, it is feasible to study the kinetics of each type of curve which represents the response to a drug application

and eventually, we can draw important conclusions about the biochemical events in the VSMC in respect to cGMP signaling.

The recorded signals (CFP, YFP, CFP/YFP) were reported for each ROI using the program associated with the epifluorescence microscope. Those signals were normalized using the frames that preceded initial drug injection.

The relative signal change (ΔR/R) was calculated according to following equation:

$\frac{\Delta R}{R} = \frac{R(t) - Ro}{Ro}$. The R_0 refers to the baseline normalization and R(t) represents the background-corrected CFP/YFP ratio:

$R_0 = \frac{1}{n} \sum_{t0}^{t1} R(t)$

$R(t) = \frac{CFP_{ROI}(t) - CFP_{bg}(t)}{YFP_{ROI}(t) - YFP_{bg}(t)}$

The index "(*t*)" indicates the time dependency of parameters. For baseline normalization, n ratio values obtained from t_0 to t_1 during the baseline period (i.e. from the start of the experiment to the first drug application) are averaged, leading to R_0. With R_0, ratio changes can be normalized to the baseline and denoted as ΔR/R. This was done automatically for all measurements via a self-made visual basic for application (VBA) script. Those ratios were plotted against time (s).

Two methods were used to evaluate the obtained data. The first was performed manually via Excel and the second one automatically through Origin. As far as the Excel evaluation is concerned (figure 2.1), the following parameters were measured:

1. "a" parameter

This indicates the time from drug application until FRET response. The latter refers to the exact time point when a rising tendency starts and was verified whenever necessary (e.g. in cells with noise) from the elevation of the CFP signal intensity and the respective decrease of YFP. This fluctuation occurs upon cGMP binding to the cGKI-derived binding sites of sensors which leads to a conformational change and to reduced FRET efficiency between CFP and YFP. It is important to note that the time span from drug application until it reaches the stage with the coverslip is 19 seconds, as it was revealed by experiment in which fluorescein-coupled BSA was applied (Lehners, Chatzieleftheriadis).

2. “c” parameter

This stands for the time from drug application until peak maximum. The peak maximum was determined by the highest point of the shaped curve that was also relatively close to the plateau of the cGMP transient.

3. “h” parameter

This represents the height from baseline to peak maximum. The height of the baseline (ΔR/R) after normalization is normally equal with 1, but this does not occur always. Hence, in case of changes in baseline between applications, a new correction of ΔR/R from the baseline to peak maximum must be taken into consideration.

4. “e” parameter

This indicates the time of “half-life” ($t_{1/2}$) of the curve as it returns from plateau back to baseline.

5 & 6. “r” and “s” parameters

The “r” parameter depicts the rising time and it is given by the equation: r = c - a, while “s” parameter stands for the slope of the curve and it is calculated as: s = $\frac{h}{r}$.

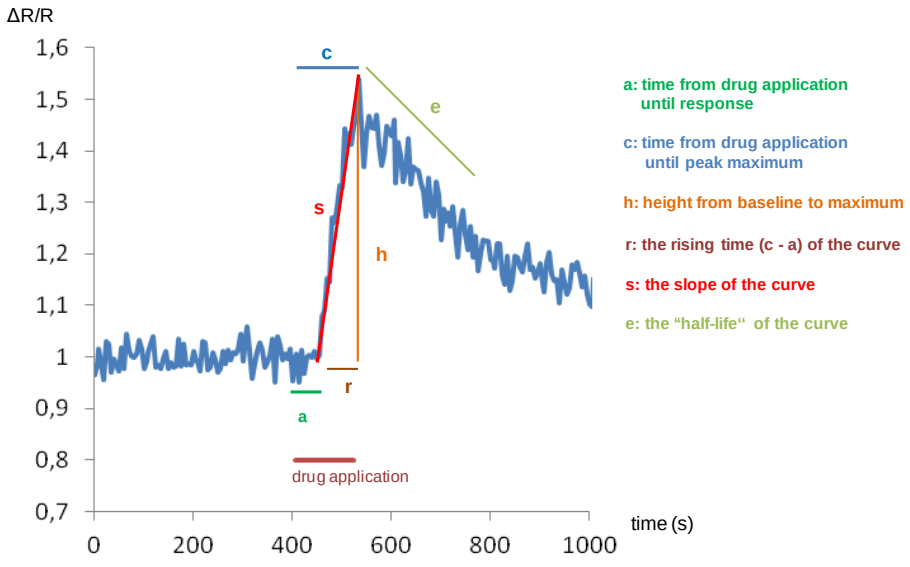

Figure 2.1. Representation of the Excel evaluation strategy.

The Origin evaluation included the “span” parameter, which is the height of the curve, and the “p” parameter which indicates the rise of the curve. Origin Pro 9

was used and the function that was utilized to fit the data, was the "Non-Linear Fitting Module". This module used a Levenberg-Marquardt algorithm for the approximation of the function to the data.

2.2.6 Immunofluorescence staining of aortic VSMCs

Immunocytochemistry and immunohistochemistry are methods to detect proteins in cells or tissue section(s), for analyzing their presence and distribution under the microscope. Immunofluorescence is a technique using fluorescent dye-labeled antibodies (Coons et. al 1942). Firstly, unlabeled primary antibodies bind specifically to their target proteins in the fixed and permeabilized cells, or tissue section(s). Fluorescent dye-labeled secondary antibodies are then used to visualize the target by binding specifically to the primary antibodies. By this method localization and co-localization studies can be performed with subcellular resolution. In the present work, secondary antibodies labeled with the fluorescent dyes Alexa Fluor 488, 555 and 594 were used (Table 2.1). The nuclei of the cells were stained to demonstrate that the cells were intact, and to estimate their number. For this purpose, the DNA-binding fluorescent dye Hoechst 33258 was used, which increases its fluorescence intensity when bound to DNA (Latt and Wohlleb 1975). BSA-PBS and Serum-PBS are used to reduce non-specific antibody binding by blocking hydrophobic binding sites (Renshaw 2007). The non-ionic detergent Triton X-100 enhances the penetration of the primary antibody by dissolving the lipid bilayer on cell membranes, nuclear membranes and organellar membranes.

Aortic VSMCs that had grown on 13-mm coverslips in 24-well plates to a confluency of 80% and that were not destined for FRET measurements, were used for immunofluorescence. Immunofluorescence staining was done to investigate the presence and expression levels of α-smooth muscle actin in VSMCs and also to visualize the distribution of cGi500 and mcGi500 in this cell type. Respectively, the Cy3 channel was used for the detection of the secondary Alexa Fluor 555 and Alexa Fluor 594 antibody (Table 2.1), while the F340 channel for the detection of Hoechst 33258.The performed protocol is the following:

1. Wash cells on coverslips in 24-wells twice with 1 mL PBS.
2. Fix cells in 1 mL ice-cold 3.7% formaldehyde in PBS solution on ice.
3. Aspirate solution.
4. Add 1 mL PBS immediately afterwards.

5. Add 2 mL BSA-PBS to a new 6-well plate, or 1.5 mL BSA-PBS to a new 12-well plate, according to the number of coverslips that are about to be analyzed.
   (The protocol from this point and on will be referring to quantities as for 6-well plates.)
6. Transfer coverslips to the new wells which contain BSA-PBS (from step 5) and incubate for 5 minutes or store coverslips at 4°C in the dark for up to 3 days.
7. Incubate for 15 minutes in 2 mL Serum-PBS with 0.2 % of Triton X-100.
8. Wash once with 2 mL BSA-PBS.
9. Place 70 µL primary antibody dilution (Table 2.1) in BSA-PBS onto parafilm.
   The parafilm should lay upon a humidified layer (e.g. wet tissue), so that the edges of the coverslip would not dry out.
10. Place the cells upside-down onto the drop carefully, by avoiding air bubble formation.
11. Incubate for 45 minutes at room temperature.
    It is also possible to incubate overnight, but this is not recommended, as drying might occur.
12. Detach coverslip carefully from the parafilm.
13. Transfer coverslips to a 6-well plate which contains 2 mL BSA-PBS with the cells facing upside.
14. Wash once with 2 mL BSA-PBS.
15. Place on parafilm a 70 µL drop of secondary antibody dilution containing 1:1000 Hoechst 33258 stock solution, diluted altogether in BSA-PBS.
16. Place the cells upside-down onto the drop carefully, by avoiding air bubble formation.
17. Incubate for 30 minutes in the dark, at room temperature.
18. Wash once with 2 mL BSA-PBS and twice with 2 mL PBS for 3 minutes.
19. Place a 50 µL drop of mounting medium (Immu-Mount, Thermo Scientific) or alternatively 40 µL of 80% Glycerol onto a microscope slide (ca. 76 x 26 mm, Roth).
    In general, the mounting medium is preferred because it provides a better clarity in observations under the microscope. The disadvantage though is that it can dry easily and cause autofluorescence. In contrast, glycerol gives less autofluorescence, but it does not dry.
20. Dip once the whole coverslip carefully for 1 second in H_2O (milliQ), to wash away PBS salts.

21. Remove excessive liquid with a tissue paper and place coverslip slowly on the mounting medium or on the glycerol drop with the cells facing towards the microscope slide, by avoiding air bubble formation.
22. Let the mounting medium dry overnight at room temperature in the dark or if you had selected glycerol, seal the edges of the coverslip carefully with a brush and nail polish, and wait for at least half an hour until it dries.
23. Examine the microscopic slides under an epifluorescence microscope after exciting at the wavelength that is appropriate for the secondary antibody, and acquire at least four representative images from each coverslip for further analysis (e.g. counting the stained cells and total cell number by counting the number of nuclei).

Table 2.1 Antibodies used in immunofluorescence. All antibody dilutions were prepared freshly. Primary antibody was diluted in BSA-PBS. Secondary antibody was diluted in BSA-PBS plus 1:1000 Hoechst 33258 stock solution.

Epitope	Type	Species	Dilution	Company/Order
mouse-SMA (monoclonal)	primary	mouse	1:1000	Sigma (A2547)
rabbit-GFP (polyclonal)	primary	rabbit	1:1000	Abcam (ab290)
rabbit-IgG-Alexa Fluor 488	secondary	goat	1:500	Invitrogen (A11008)
mouse-IgG-Alexa Fluor 555	secondary	goat	1:500	Invitrogen (A21424)
rabbit-IgG-Alexa Fluor 594	secondary	goat	1:500	Invitrogen (A11012)

2.2.7 Protein transduction of transgenic cells via HTNC

Protein transduction is a process which relies on the inherent property of a small number of proteins and peptides of being able to transverse the cell membrane (Morris, Depollier et al. 2001). It has been demonstrated that small parts of these proteins (10–16 amino acids in length) are responsible for this phenomenon. Linking these domains covalently to compounds, antisense peptide nucleic acids, peptides,

or in-frame fusions with full-length proteins, enables them to enter the lipid bilayer of any cell type in a transporter and receptor-independent manner (Schwarze, Ho et al. 1999).

Recombinant Cre recombinase HTNC (His-TAT-NLS-Cre) is derived from E. coli bacteria carrying an engineered plasmid encoding Cre recombinase from bacteriophage P1 with additional N-terminal 6xHis tag, a TAT peptide and a NLS sequence. This cell-permeant Cre recombinase (HTNC) is considered the most effective protein in transduction and subsequent recombination compared to other forms of Cre recombinases (Peitz, Pfannkuche et al. 2002). The efficiency of the protein transduction depends also on the cell confluency which should be at least 80% as well as on the cell culture conditions which precede the procedure (see protocol; step 2). The protocol mentioned below is as for each well of a 24-well plate:

1. Wash once with 1 mL pre-warmed PBS.
2. Incubate cells with serum-free medium (480 µL) 2-4 hours prior to HTNC transduction.
   This step can enhance the efficiency of the method.
3. Dilute 2.8 µL of HTNC protein stock into 480 µL of serum-free medium in a 1.5 mL Eppendorf tube.
4. Tap the tube to mix well and centrifuge for 30 seconds to allow precipitation at the bottom.
5. Remove serum-free medium from the well of interest.
6. Take 450 µL of supernatant from the Eppendorf tube, avoiding precipitate aspiration, and add to the respective well.
7. Place 24-well plate in the incubator for 8-20 hours.
8. Wash twice with serum-free medium.
   Washing with PBS is not recommended as it could increase the stress that the cells are undergoing.
9. Change medium into normal cell culture medium (DMEM with 10% FBS).
   This step can enhance the rate of proliferation and therefore may increase the number of the transduced cells.
10. Results are safe to be observed and obtained in the epifluorescent microscope 2-4 hours later.

2.2.8 Subcellular fractionation

Subcellular fractionation is a method that provides the required means to analyze the properties and composition of purified cellular components. Subcellular fractionation by differential centrifugation was first described by De Duve and colleagues (De Duve, Pressman et al. 1955) and has subsequently been the method of choice for isolating cell organelles from various tissues and cultured cells.

Subcellular fractionation was used for aortic VSMCs expressing either mcGi500 or cGi500 biosensor, and the ultimate goal was to investigate the distribution of each sensor in the cytosol, membrane, and nucleus. The performed protocol is the following (all centrifugations were done at 4^{o}C):

1. Remove medium from plates (145 x 20 mm, Cellstar) with cells and wash once with PBS.
2. Lyse cells on plates using 500 µL of subcellular fractionation buffer. Scrape plates immediately with a cell scraper and place the homogenized cell extract in a 1.5 mL Eppendorf tube.
3. Then pass lysate through a 26 Ga needle 10 times using a 1 mL syringe.
4. Leave on ice for 20 minutes.
5. Centrifuge at 3000 rpm for 5 minutes. The nuclear pellet should be washed once by adding 500 µL of fractionation buffer again. Disperse the pellet with a pipette and pass through a 26 G needle 10 times.
6. Centrifuge again at 3000 rpm for 15 minutes. Remove the wash buffer, and resuspend the nuclear pellet in the nuclear buffer (standard lysis buffer with 10% glycerol and 0.1% SDS added). Sonicate nuclear pellet briefly (for 3 seconds) on ice.
7. Remove supernatant and place it in a fresh 1.5 mL Eppendorf tube.
8. Centrifuge the supernatant again at 8000 rpm. Remove the supernatant again. This is the cytosolic and membranic fraction.
9. For a membranic fraction: centrifuge the supernatant in an ultracentrifuge (Beckman TL-100 Ultracentrifuge) in a special Eppendorf tube (9.5 x 38 mm, Microfuge Tube Polyallomer). Centrifuge at 41,000 rpm for 1 hour. Remove the cytosolic fraction as supernatant and place it in a fresh, normal 1.5 mL Eppendorf tube. Wash pellet as by adding 400 µL of the fractionation buffer to the pellet. Resuspend by pipetting. Use a 26 G needle as above. Then re-centrifuge for 45 minutes. Resuspend the membrane pellet in the same buffer as used for the nuclei.
10. Store samples at -20^{o}C.

2.2.9 Protein Analysis

2.2.9.1 Protein precipitation

2,2,2-Trichloroacetic acid is an analogue of acetic acid firstly synthesized by Jean-Baptiste Dumas in 1839. TCA-induced protein precipitation is the most popular and preferred method for sample preparation regarding proteome analysis [(Nandakumar, Cheung et al. 2006); (Jacobs, van Rijssen et al. 2001)]. Protein precipitation with TCA is an instantaneous, simple, and efficient process which is also performed to remove a buffer or a substance out of the sample of interest, or to concentrate samples (e.g. for SDS-PAGE). The mechanism of this method is based on the fact that negatively charged trichloroacetate ions trigger protein unfolding by intervening with the electrostatic interactions that stabilize the native conformation of proteins. This partial unfolding of proteins results in the exposure of solvent-accessible non-polar surfaces, which consequently results in intermolecular coalescence of protein molecules leading ultimately to their precipitation (Rajalingam, Loftis et al. 2009). An ideal method for protein extraction should reproducibly capture the most comprehensive repertoire of proteins possible, with no or very minimal degradation and contamination by non-proteinaceous compounds (Harder, Wildgruber et al. 1999). The disadvantage of this method is that unfolded/denatured proteins have a lower tendency to precipitate in TCA.

This method was used to precipitate the proteins present in the fractions of cytosol, membrane and nucleus, and also to eliminate any reducing substance that could interfere with the Lowry assay. The TCA-induced protein precipitation protocol is the following:

1. Add 1 volume of TCA stock to 4 volumes of protein sample.

   i.e. in 1.5 mL tube, add 250 µL TCA to 1 mL sample.

2. Incubate for 10 minutes on ice.

3. Centrifuge tube(s) at 14.000 rpm for 15 minutes at 4^{o}C (Centrifuge 5417R, Eppendorf).

4. Remove carefully the supernatant, leaving protein pellet intact. Pellet should be whitish and turbid.

5. Wash pellet with 200 µL cold acetone.

6. Centrifuge tube(s) again at 14.000 rpm for 15 minutes at 4^{o}C.

7. Repeat steps 4-6 for a total of 2 acetone washes.

8. Dry pellet by placing tube in 95^{o}C heat block (Thermomixer compact, Eppendorf) for 8 minutes to drive off acetone.

9. Add protein buffer (Thunemann, Wen et. al 2013).

2.2.9.1 Protein Quantification

The protein concentration of subcellular components was determined using the Peterson's modification of the Lowry method [(Lowry, Rosebrough et al. 1951); (Peterson 1977)]. The Lowry protein assay consists of two reactions: The first one is based on the biuret test in which cupric ions bind with peptide bonds of the proteins under alkaline conditions (Lowry Reagent Solution). In the second reaction (Folin Ciocalteu's Phenol Reagent Working Solution) which is under acidic conditions, electrons are transferred from the cupric ion peptide complex to molybdenum ions which are thereafter reduced to molybdenum blue. This blue colored solution can be measured photometrically and directly correlates with the protein content of the sample. Finally, the protein concentration can be determined using a calibration curve.

The advantage of the Lowry method is the insensitivity to detergents such as SDS, which is contained in the lysis buffer and thus in the protein lysates. On the other hand, the sample has to be free from any reducing agent, which would disturb the Lowry assay. Therefore, it must be performed after TCA precipitation.

The protein quantification was performed to permit equal loading of protein for SDS-PAGE and for Western blot afterwards, to facilitate the comparison of different protein samples. The Micro-Lowry-Total-Protein-Kit (Sigma) was used. BSA standard controls were prepared and the used concentration was 12.5 µg/mL, 25 µg/mL, 50 µg/mL, 100 µg/mL, and 200 µg/mL. As a negative control, H_2O (milliQ) was used. All protein determinations were performed double at room temperature.

1. Add separately in a 96 well plate, 10 µL of protein sample(s) diluted with 90 µL H_2O and 100 µL of each BSA standard.
2. Prepare negative controls; 90 µL H_2O along with 10 µL of particular lysis buffer in which the protein samples are diluted and separately 100 µL H_2O.
5. Add 100 µL Lowry Reagent Solution in each well of interest.
6. Vortex briefly for 2 seconds and incubate in the dark for 20-30 minutes at room temperature.
7. Add 50 µL of Folin Ciocalteu's Phenol Reagent Working Solution.

8. Vortex briefly for 2 seconds and incubate in the dark for 45 minutes at room temperature.
9. Read absorption at 620 nm in a spectrophotometer (Multiskan EX, Thermo Scientific).
10. Plot the optical density (OD 620) against the BSA concentration, fit a linear regression analysis, and calculate the desired concentrations of the protein samples.

2.2.9.2 SDS-PAGE

The separation of macromolecules in an electric current is called electrophoresis. A common method for separating proteins by electrophoresis uses a discontinuous polyacrylamide gel as a support medium and sodium dodecyl sulfate (SDS) gel to denature the quaternary, tertiary and secondary structure of proteins. The method is called sodium dodecyl sulfate polyacrylamide gel electrophoresis (SDS-PAGE) (Laemmli 1970). The proteins in SDS-PAGE are separated according to their electrophoretic mobility which is dependent on their size. To be specific, the negatively charged SDS molecule binds in a ratio of approximately 1 molecule per 2 amino acids, which leads to a negative charge which is proportional to the unique mass of a protein.

The proteins which are represented in bands can be visualized afterwards via coomassie staining. The loading buffer contains β-mercaptoethanol for reducing conditions.

2.2.9.2.1 Preparation of Polyacrylamide Gels

The polyacrylamide gels were prepared using the Mini PROTEAN 3 System (BioRad). The gels were used in a thickness of 1.5 mm and the recipe is given below (Table 2.2). The 8% gels were prepared for the proteins of interest. Gels were prepared as following:
1. Clean glass plates with soap and later with 70% ethanol thoroughly and let dry.
2. Clamp glass plates in the Mini PROTEAN 3 System rack and test with H_2O (milliQ) to detect any leakage. In that case, reassemble firmly the glass plates in the rack.
3. Prepare resolving gel solution, add TEMED and APS lastly.
4. Pour solution between the glass plates with a pipette facing vertically, up to maximum 2 cm beneath the upper rim.
5. Overlay solution with 1 mL isopropanol and allow polymerization for 20 minutes.

6. Remove isopropanol thoroughly and allow the gels to dry.
7. Prepare stacking gel solution, add TEMED and APS lastly.
8. Place until top the stacking gel solution and place combs immediately afterwards.
9. Allow polymerization and wait for 40 minutes.
10. Remove combs and use the gel or wrap altogether the glass plates with gel and comb in a wet tissue paper, and later wrap with cling film to maintain humidity. Finally, store at 4^{o}C until future use (approx. up to 1 week).

Table 2.2. Composition of polyacrylamide gels. The given amounts are adequate for two 0.75 mm gels. A ready-to-use aqueous 30% acrylamide and bisacrylamide stock solution at a ratio of 37.5:1 (Rotiphorese Gel30, Roth) was used; TEMED (Roth) and APS should be added at last.

Reagents	**Resolving gel**	**Resolving gel**	**Stacking gel**
	12%	**8%**	**4%**
Rotiphorese	4 mL	2.7 mL	0.65 mL
4×resolving gel buffer	2.5 mL	2.5 mL	-
4×stacking gel buffer	-	-	1.25 mL
TEMED	10 µL	10 µL	10 µL
APS (20%)	50 µL	50 µL	50 µL
H_2O (milliQ)	3.4 mL	4.7 mL	3.05 mL

2.2.9.2.2 Separating proteins through SDS-PAGE gel

1. Add 5x Lämmli SDS loading buffer to the protein samples.
2. Incubate for 5 minutes at 95^{o}C and centrifuge briefly.
4. Install gels in the gel running chamber, fill with SDS running buffer, take out the comb and wash the loading wells.
5. Load gels with the supernatant of the protein samples; load 2-5 µg protein per well and 3 µL of marker (PageRuler Plus Prestained Protein Ladder, Fermentas).
6. Start running gel with 100 V until running dye front (bromophenol blue) enters the resolving gel, then switch to 150 V.
7. Stop gel after approx. 40 minutes, when the running dye front runs out.
8. Disassemble the gel chamber, separate the stacking from the running gel and discard the stacking gel.
9. Use gel for Coomassie staining or for Western blot.

2.2.10 Confocal Laser Scanning Microscopy (CLSM)

Confocal microscopy is a powerful tool for visualization and quantification of three-dimensional structures. The basic concept of confocal microscopy was originally developed by Marvin Minsky (Minsky 1961). Modern confocal microscopes are now considered as integrated electronic systems where the optical microscope plays a central role in a configuration that consists of one or more electronic detectors, a computer (for image display, processing, output and storage), and several laser systems combined with wavelength selection devices and a beam scanning assembly. These microscopes are now being employed for investigations on molecules, cells, and living tissues that were not possible few years ago.

Confocal microscopy offers several advantages over conventional widefield optical microscopy, including the ability to control depth of field, elimination or reduction of fluorescence emission from regions removed from the focal plane which is the main cause for quality degradation in the image, and the capability to collect serial optical sections from thick specimens. The consequent result is the drastical improvement of contrast providing enhanced clarity.

Briefly, the basic tools in a CLSM are the following (Claxton 2006):

1. Laser
   It is the illumination source which excites the fluorophores of a specimen. It can be focused by the lens system to a very small spot at the focal plane. The sample can be protected from photobleaching by lowering its intensity.
2. Scanner
   The image of a specimen can be generated by scanning the focused beam across a defined area in a raster pattern controlled by two high-speed oscillating mirrors driven with special galvanometer motors. One of the mirrors moves the beam from left to right along the *x* lateral axis, while the other translates the beam in the *y* direction.

3. Z-control

   It provides the ability to focus into a specimen and acquire layer images X-Y through the *z* axis, as well as regulation of parameters such as the of size of moving step towards the *z* axis.

4. Pinhole

   It is a very important tool as it can exclude fluorescence signals from out-of-focus features positioned above and below the focal plane. It also serves to eliminate much of the stray light passing through the optical system.

5. Photomultiplier (PMT)

   These low-background photomultipliers are able to detect protons which are emitted by the reflection of the specimen after illumination.

6. Dicroic Beam Splitter

   It determines the route of the fluorescent rays and it is determined by a combination of basic (HFT) and secondary dicroic mirrors (NFT) and excitation filters.

   HFT: separates the excitation light from the emission light,

   NFT: separates the emitted fluorescence; e.g. NFT 545 mirror reflects light in wavelength lower than 545 nm and permits the light in wavelength higher than 545 nm to pass through.

7. Objective lens

   It determines the magnification of the specimen, as well as the resolution of an acquired image which is dependent upon the light intensity.

In the current study, CLSM imaging was performed on a Zeiss LSM 510 META, with living VSMCs incubated with or without Hoechst 33258 dye (1:250), 1 hour prior of the beginning of the experiment. The executed steps were the following:

1. Mount the coverslips with cells on the stage and use the 63x/1.4 lens which is covered on top with a drop of oil (Immersol 518 F, Zeiss), to ensure light intensity.
2. Install the laser and the wavelength of interest (e.g. Argon/2, 488 nm for EGFP) and set up the intensity of laser light (5-25%).

   Consider that the laser can cause photo-bleaching of the sample and therefore a low intensity should be used.
3. Excite in the appropriate wavelength and detect a region of interest, via epifluorescence.
4. Select the suitable reflectors and dicroic mirrors (e.g. NFT 490).

5. Select “Fast XY” to perform continuous fast scanning, while the “Detector Gain” is on and arranged in the range of interest.
   The “Fast XY” is useful for finding and changing the focus. The resolution is dependent upon the “Detector Gain”. The latter option determines the sensitivity of the detector by setting the maximum limit.
6. Arrange “Z-stack”.
7. Select upper/lower focus and arrange “step size”.
8. Set up other parameters such as the number of slices to increase the signal to noise ratio.
9. Close pinhole to 1 arb. unit, before you start acquiring a confocal image.
10. Wait a few minutes as the scanning process is running, and later observe and save the obtained confocal image.

3 Results

3.1 Immunocytochemistry of transgenic VSMCs from the aorta

VSMCs expressing either cGi500 or mcGi500, were isolated from the aorta of transgenic mice (R26-CAG-cGi500 and R26-CAG-mcGi500, respectively) and analyzed as a part of this research. Their morphology is clear enough to be observed and distinguished in respect to the sensor type, when using 40x magnification in an epifluorescence microscope. Considering the 3D structure of a cell, VSMCs expressing the cGi500 biosensor can be distinguished from the cells expressing mcGi500 by the fact that in the first case, the nucleus is more obvious as the fluorescence deriving from the expression of cGi500 sensor, is located to the cytosol, whereas in the case of mcGi500, the fluorescence is more dim because the sensor is distributed in the membrane and therefore the inner part of the cell is hardly visible.

VSMCs differ from other types of SMCs such as those from the digestive or the urogenital tract, by the fact that α-smooth muscle actin is predominantly expressed in VSMCs (Gabbiani, Schmid et al. 1981). It has also been reported that the expression levels of this protein, remain in high levels in the contractile state of the VSMC and they are reduced during phenotype switch (Rensen, Doevendans et al. 2007). Thus, antibody for α-smooth muscle actin can be used as a marker for the detection of contractile VSMCs.

In the following figures, immunofluorescence staining of primary VSMCs expressing either cGi500 or mcGi500 is presented. Firstly, immunocytochemistry was performed for the detection of α-smooth muscle actin. VSMCs were grown in normal cell culture medium (DMEM with 10% FBS) for 8 days and in serum-free medium for 2 additional days. It was found that 55% of cells deriving from mixed mcGi500/cGi500 VSMC culture were α-smooth muscle actin-positive (figure 3.1, A) and 59% of mcGi500 VSMC culture were α-smooth muscle actin-positive (figure 3.1, B). The proportions come from the average out of 4 calculations in different fields of view and are in accordance with previous observations (M. Thunemann).

(A)

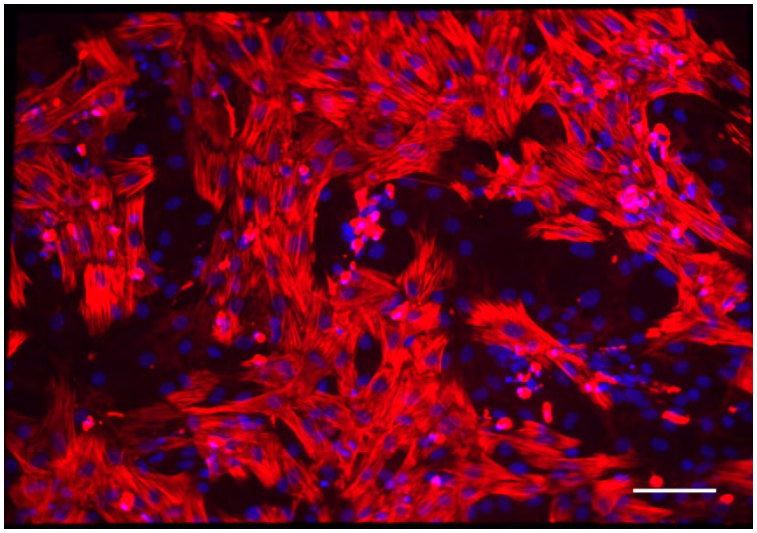

(B)

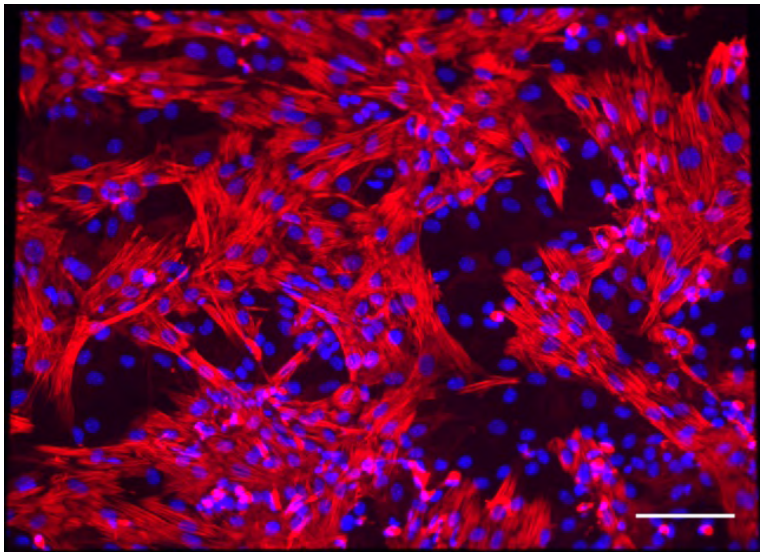

Figure 3.1. Immunofluorescence for the detection of α-smooth muscle actin in aortic VSMCs expressing mcGi500 and cGi500. Primary antibody: monoclonal anti-α (mouse) smooth muscle actin. Secondary antibody: Alexa Fluor 555 anti-mouse IgG (H+L) (red), and Hoechst 33258 for nuclear staining (blue). (A) Representative image of mcGi500- and cGi500-VSMC mixed culture. (B) Representative image of mcGi500-VSMC culture. The images were obtained at 40x magnification. Scale bars: 35 μm.

Immunofluorescence staining was also performed for the detection of cGi500 and mcGi500 by using an anti-GFP antibody, so that we would observe the distribution of the fluorescence via epifluorescence microscopy, after the immunostaining process (figure 3.2, right side). The endogenous fluorescence of both sensors expressed in VSMCs was partially or fully diminished after staining (figure 3.2, left side). The percentage of EGFP-positive VSMCs was 100%, as it was examined in 5 different fields of view.

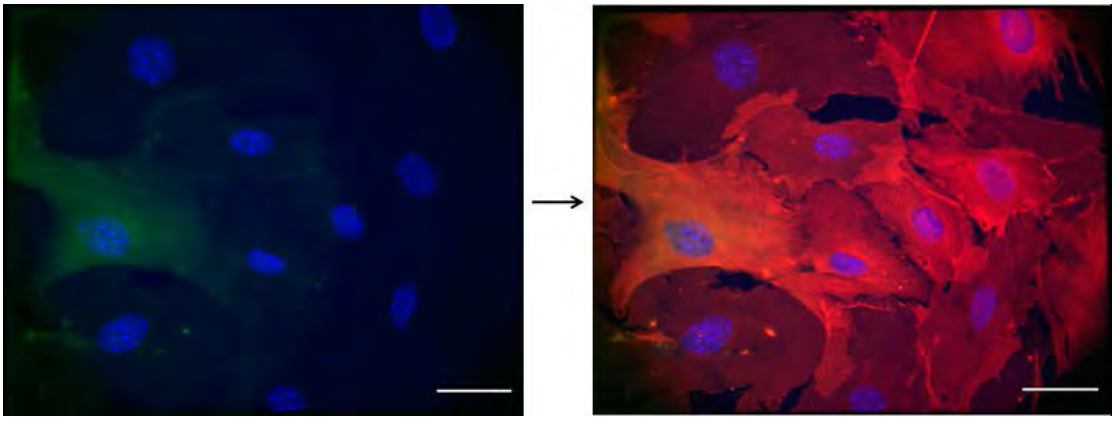

Figure 3.2. Immunostaining of mcGi500- and cGi500-VSMCs in the absence (left side) and presence (right side) of polyclonal anti-GFP primary antibody (rabbit) and secondary Alexa Fluor 594 anti-rabbit IgG (H+L) (red). Hoechst 33258 was used for nuclear staining (blue). The endogenous fluorescence (green) of sensors (left side) was detected in the YFP channel after the immunostaining process. The images were obtained at 40x magnification. Scale bars: 35 µm.

3.2 Localization of mcGi500 and cGi500 in subcellular compartments

The cGMP FRET biosensors mcGi500 and cGi500 may be useful research tools to study in real-time the cGMP levels within living cells after application of a specific substance. In principle, the mcGi500 biosensor is designed to be localized specifically to the membrane, while cGi500 lacks this ability. What makes the difference for mcGi500 is the expression of eight additional amino acids (Met-Gly-Cys-Cys-Phe-Ser-Lys-Thr) from the MARCKS protein (Myristoylated Alanine-Rich Protein Kinase C Substrate) that is endogenously localized to the plasma membrane.

This localization occurs due to hydrophobic interactions of the N-terminal myristoyl moiety with the membrane (Manenti et. al 1999). Myristoylation refers to the attachment of a C14 saturated fatty acid (myristate) to the N-terminal glycine of substrate proteins. The soluble enzyme N-myristoyl transferase transfers a myristoyl moiety from the cofactor myristoyl-CoA to the N-terminus of nascent proteins containing the consensus sequence (Gly-*X*-*X*-*X*-Ser/Thr) (Johnson et al., 1994). The first eight amino acids of the MARCKS protein are essential for this process. The myristoyl moiety mediates insertion into the lipid bilayer and thereafter the sensor is able to be localized to the membrane.

It was a subject of interest to verify if this kind of localization of mcGi500 does indeed take place in aortic VSMCs, and also to investigate eventually the exact localization of cGi500 in subcellular compartments. For these purposes, two strategies were put in application. In the first case, VSMCs expressing each sensor had been passaged twice and seeded separately in cell culture dishes (100 mm x 20 mm, Corning), until they reached at least 80% confluency. Then, subcellular fractionation was performed, and the obtained fractions for the nucleus, the cytosol, and the membrane were destined for Western blot analysis. The basic idea was to use for every fraction, antibodies that detect proteins embedded in the membrane, antibodies for the detection of proteins in the cytosol and EGFP antibodies which detect the cGi-type biosensors. Then, the results would provide important information about the localization of each sensor.

Preceding Western, protein analysis of the samples for the different fractions had to be performed. The TCA protein precipitation method was performed to remove the reagent DTT that was present in the buffer of samples, and to concentrate them. Lowry assay was performed and the results showed that the concentration of proteins in the membranic and nuclear fraction was considerably low (~ 0.03, 0.025 mg/mL respectively), while the concentration of the cytosolic one was normal (~ 0.2 mg/mL). SDS-PAGE and Coomassie staining were performed and from the results which are shown below (figure 3.3), we would decide if it was feasible to continue with the Western blotting assay. Finally, the experiment was recommended to end at that point, without proceeding with Western blotting, as the membranic and the nuclear fraction reported absent or very weak signal, after SDS-PAGE and staining with Coomassie.

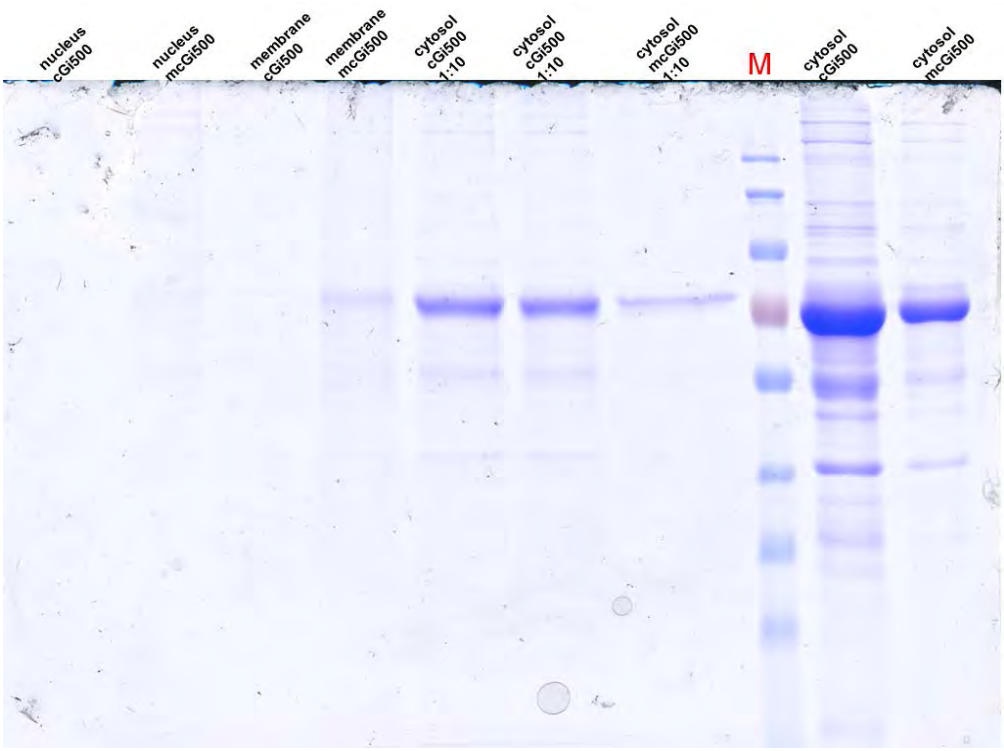

Figure 3.3. Coomassie stained polyacrylamide gel (8%) after SDS-PAGE protein separation of fractions deriving from the cytosol, the membrane, and the nucleus of aortic VSMCs expressing either mcGi500 or cGi500 biosensor. “1:10” represents the dilution of the samples with loading buffer and “M” stands for the pre-stained molecular weight marker.

In the meantime, there was also another strategy that seemed more direct and promising than the previous one. This was to obtain images of living cells by confocal microscopy, to observe in depth the fluorescence of each biosensor and therefore draw safe conclusions about its distribution. The primary advantage of laser scanning confocal microscopy over epifluorescence microscopy is the ability to produce thin (0.5 to 1.5 μm) optical sections through fluorescent specimens. A set of two-dimensional (2D) confocal images that were obtained sequentially inside the specimen, were combined and resulted in a three-dimensional (3D) fluorescent image of the cell (figure 3.5).

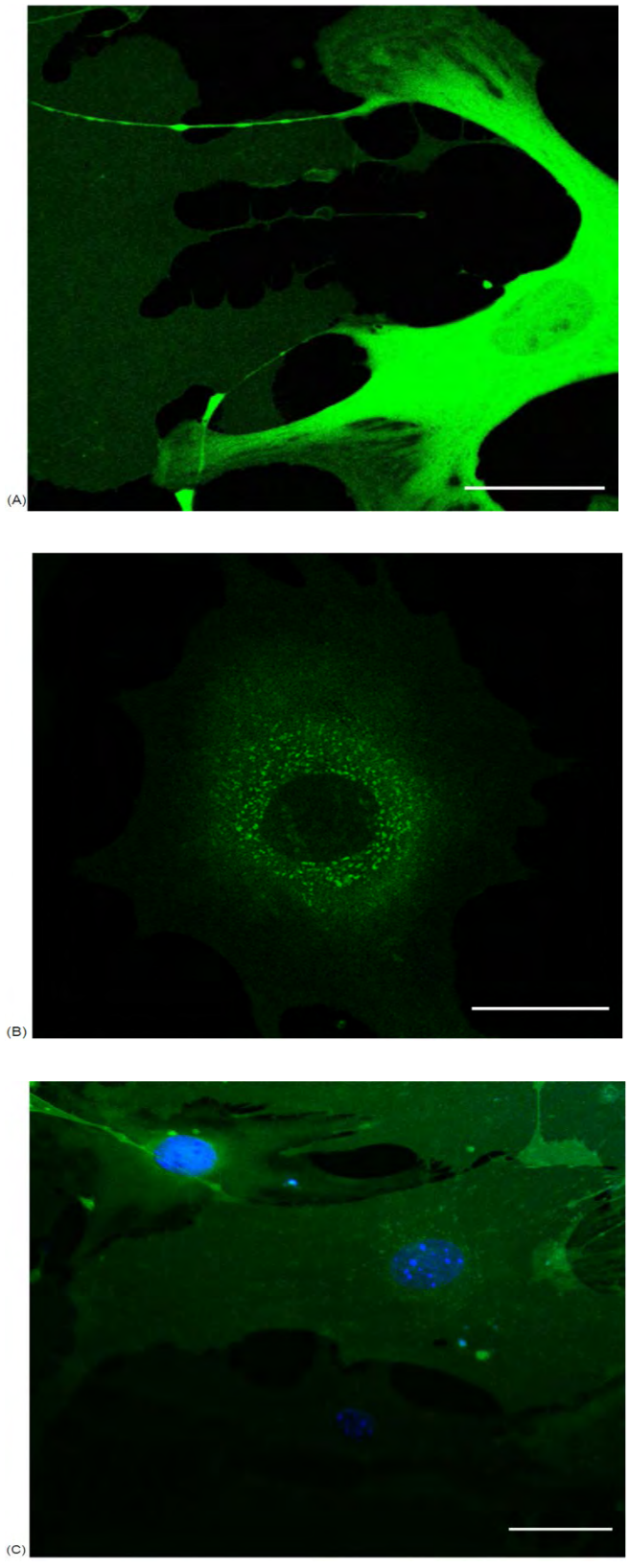

Figure 3.4. Images of living VSMCs obtained with confocal laser scanning microscopy. (A) VSMCs expressing the membrane-bound mcGi500 (left) and cytosolic cGi500 (right) biosensor. (B) VSMC expressing the mcGi500 biosensor; the nucleus and vesicles that were transporting mcGi500 protein molecules to the membrane, can be observed. (C) VSMCs

expressing mcGi500 sensor, pre-incubated with Hoechst 33258 for nuclear staining (blue). The images were obtained at 64x magnification. Scale bars: 35 μm.

From the results (figures 3.4, 3.5), it was made obvious that mcGi500 was located indeed in the membrane; for instance, the cross-section below (figure 3.5) indicates that the fluorescence of the sensor (i.e. mcGi500 localization) is almost absent inside the VSMC. In contrast, the fluorescence deriving from cGi500 was found to be located in the cytosol in much higher levels than mcGi500. cGi500 expression was observed also in the nucleus, but at lower levels than in the cytosol.

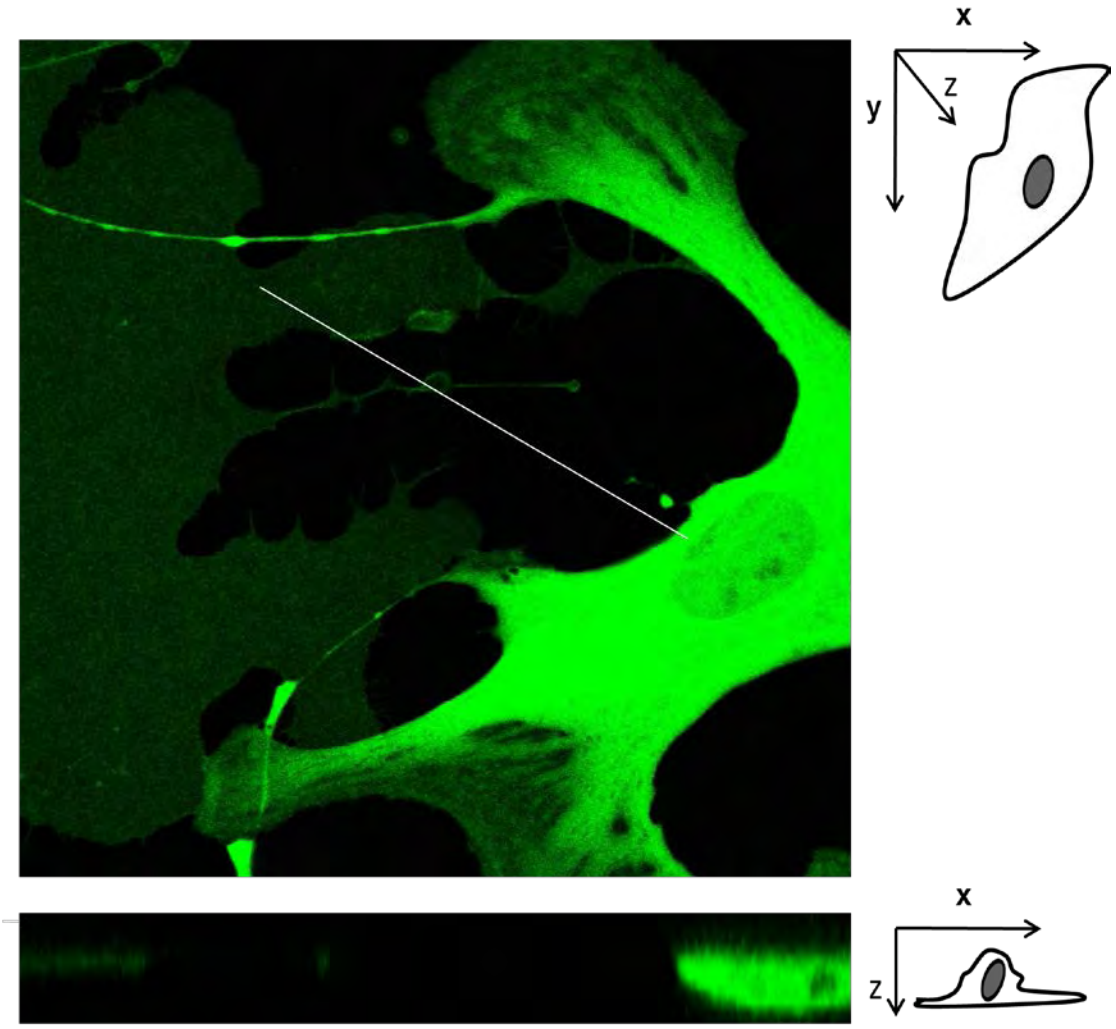

Figure 3.5. Confocal 3D image of aortic VSMCs expressing mcGi500 (left) and cGi500 (right). The white line indicates the performed cross-section, and at the bottom there is the result of the section as it is observed from the side of the cells. It is also illustrated the orientation of the specimen in respect to x,y and z axis (right side). The ultimate height of the VSMC (right) onto the coverslip was found to be 6 μm.

3.3 General responses of VSMCs from the aorta, to ANP, CNP & DEA/NO

In general, aortic VSMCs express both GC-A and GC-B receptors, as well as the sGC receptor. ANP, CNP and the nitric oxide donor DEA/NO were used as part of this research, to activate the catalytic domain of those receptors, respectively. Examining how the aortic VSMCs respond to each activator is an important aspect of this study.

The responses of primary VSMCs from the aorta, after ANP, CNP, and DEA/NO application, were measured in living cells and in real-time, by utilizing the FRET principle. Either of two biosensors was expressed in these cells: the cGi500 which is predominantly expressed in the cytosol and the mcGi500 which is a membrane-bound biosensor. The responses are presented as curve formations, which depict the change of CFP/YFP ratio relative to the baseline (ΔR/R).

After FRET experiments, the results were evaluated via Excel and Origin. The two evaluation strategies were performed to compare the calculated results with each other, and then select the most accurate parameters for the comparison of the cGi500 and mcGi500 sensors. One method seemed to overlap the weaknesses of the other. Paradigm of a positive correlation between the two methods of evaluation is depicted below (figure 3.6). Finally, the selected parameters presented in this study, were “a”, “c”, and “h” parameters from Excel, as well as the “p” parameter calculated via Origin.

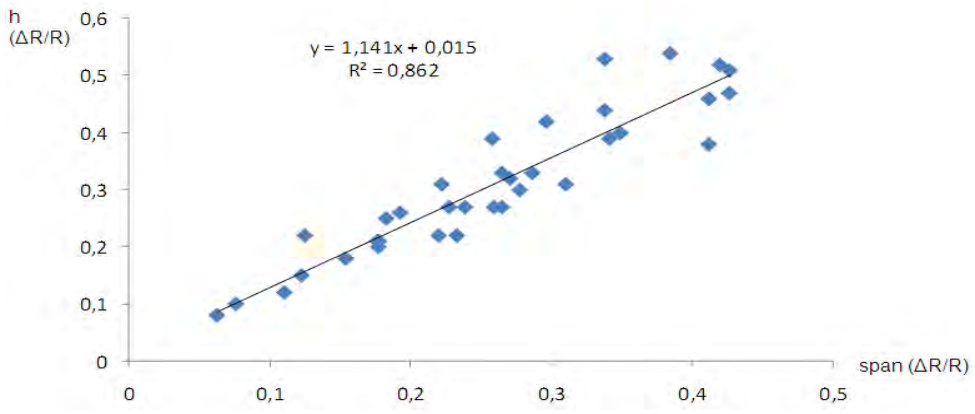

Figure 3.6. Comparison between peak height “h” (*y* axis) and “span” (*x* axis) parameters from the same measurement, as they were calculated via Excel and Origin, respectively. The illustrated R^2 value indicates a close correlation between the calculated parameters.

Results from the data evaluation demonstrated that VSMCs do not respond in the same manner for each cGMP-elevating agent (ANP, CNP or DEA/NO). To be

specific, cells exhibited weak, mild, strong, or even absent responses after application of ANP (figure 3.7). The same phenomenon was observed also for CNP. What is more, absent responses seem to be independent of the drug concentration (figure 3.8). In contrast, responses to DEA/NO were predominantly strong and only a minority (5%) of the examined VSMCs did not respond; specifically, only 6 out of 120 examined cells, in 17 relative experiments, did not react to DEA/NO. However, even if most of the DEA/NO responses were strong, there was not a particular pattern in the kinetics and the shape of the respective curves in all cases (figure 3.9).

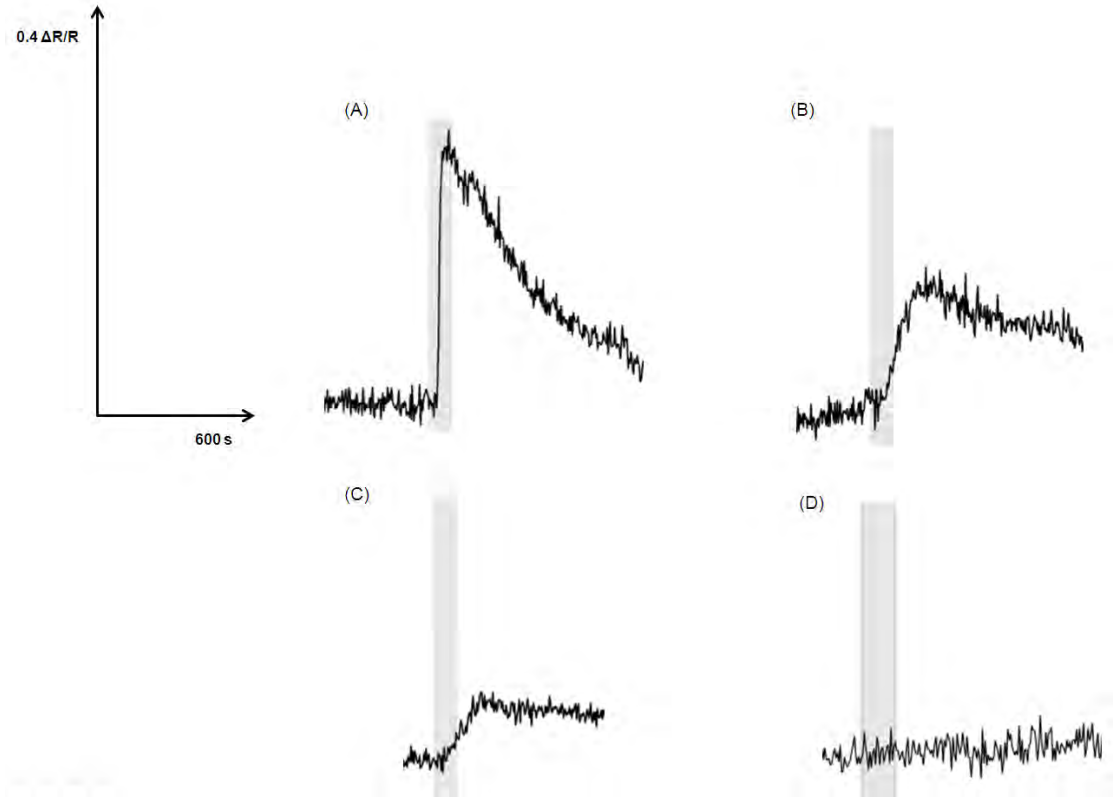

Figure 3.7. Representative examples of the variability in the strength of FRET cGMP responses in VSMCs, after ANP application: (A) strong , (B) mild, (C) weak, and (D) absent responses. The concentations of ANP which were used are the following: (A), (B) 85 nM, (C) 170 nM and (D) 100 nM. The examples derive from responses of cGi500-expressing VSMCs. The grey rectangles indicate the drug application.

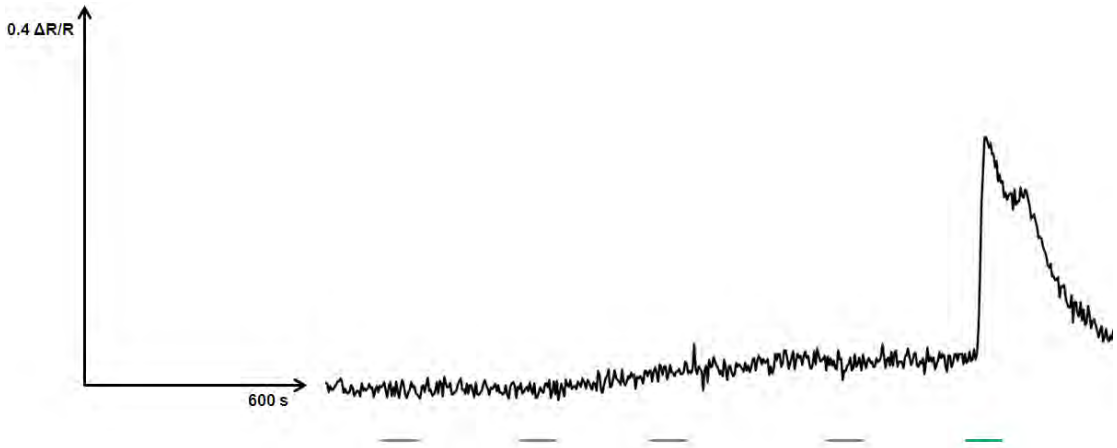

Figure 3.8. Absence of response in elevating concentrations of CNP, regarding a single VSMC (sensor: mcGi500). The grey bars indicate the application of CNP, in the order of following concentrations: 16, 33, 50 & 75 nM. The green bar indicates the induced response to DEA/NO (100 nM).

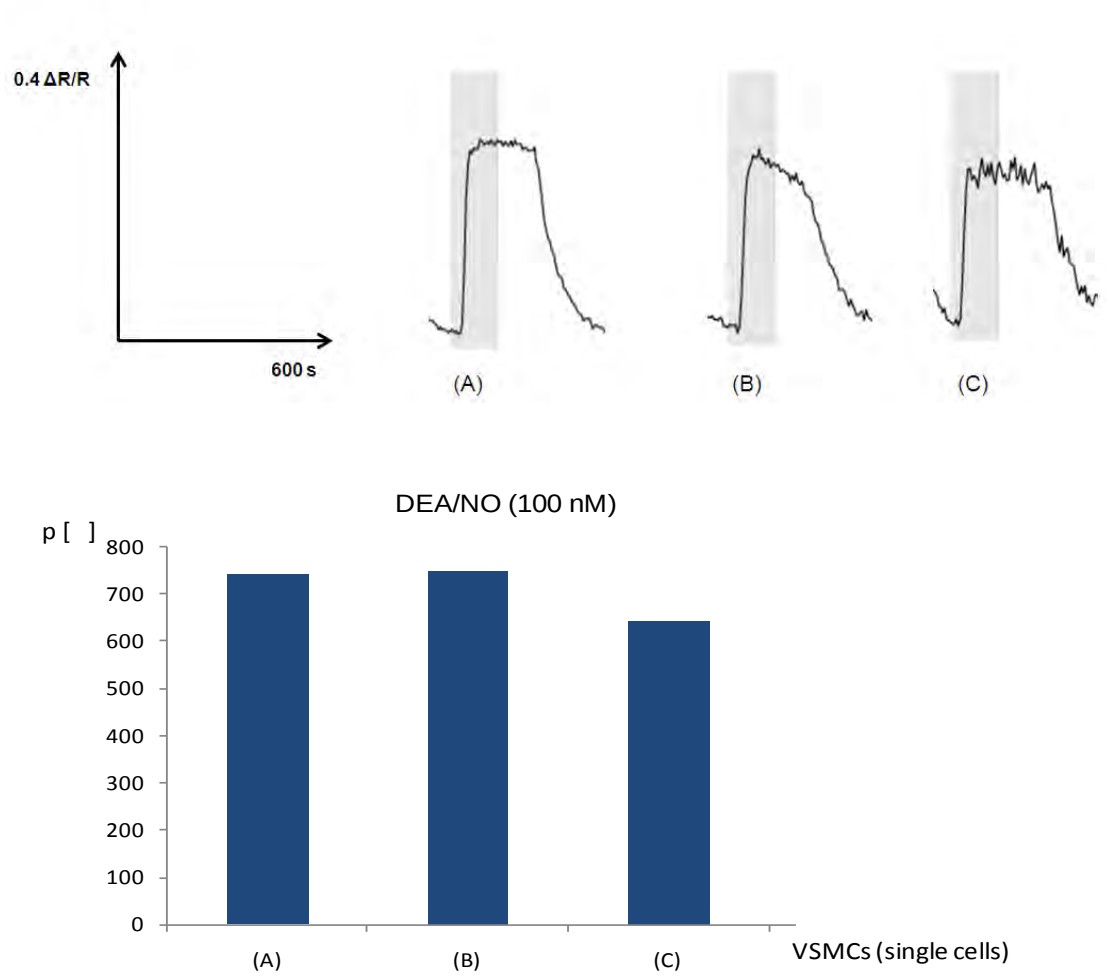

Figure 3.9. Diversity in curve shape and kinetics between aortic VSMCs regarding DEA/NO responses in a representative experiment. The three curves (upper side) stem from responses of 3 different VSMCs to DEA/NO (100 nM) in the same experiment; (A), (B)

mcGi500, and (C) cGi500 are the expressed cGMP FRET biosensors. The grey rectangles indicate the drug application. The studied “p” parameter (lower graph) represents the rise of each curve, as it was calculated via Origin.

In dose-response experiments, aortic VSMCs exhibited a different behavior after being exposed to elevating concentrations of ANP, CNP and DEA/NO. This behavior can be easily distinguished and compared by eye (figure 3.10). VSMCs responded generally stronger to each rising concentration of CNP (figure 3.10, B). However, the same phenomenon was not observed for the VSMCs which had been stimulated and reacted to ANP in another relative experiment (figure 3.10, A). Finally, the cells which were treated in rising concentrations of DEA/NO displayed an acute response already at the initial drug application and it seemed that there was only a slight change in the characteristics of the curves in-between the various drug applications (figure 3.10, C). However, the examination of the data of the latter experiment demonstrated increases in the p parameter of those curves, as the DEA/NO concentration was rising (figure 3.11).

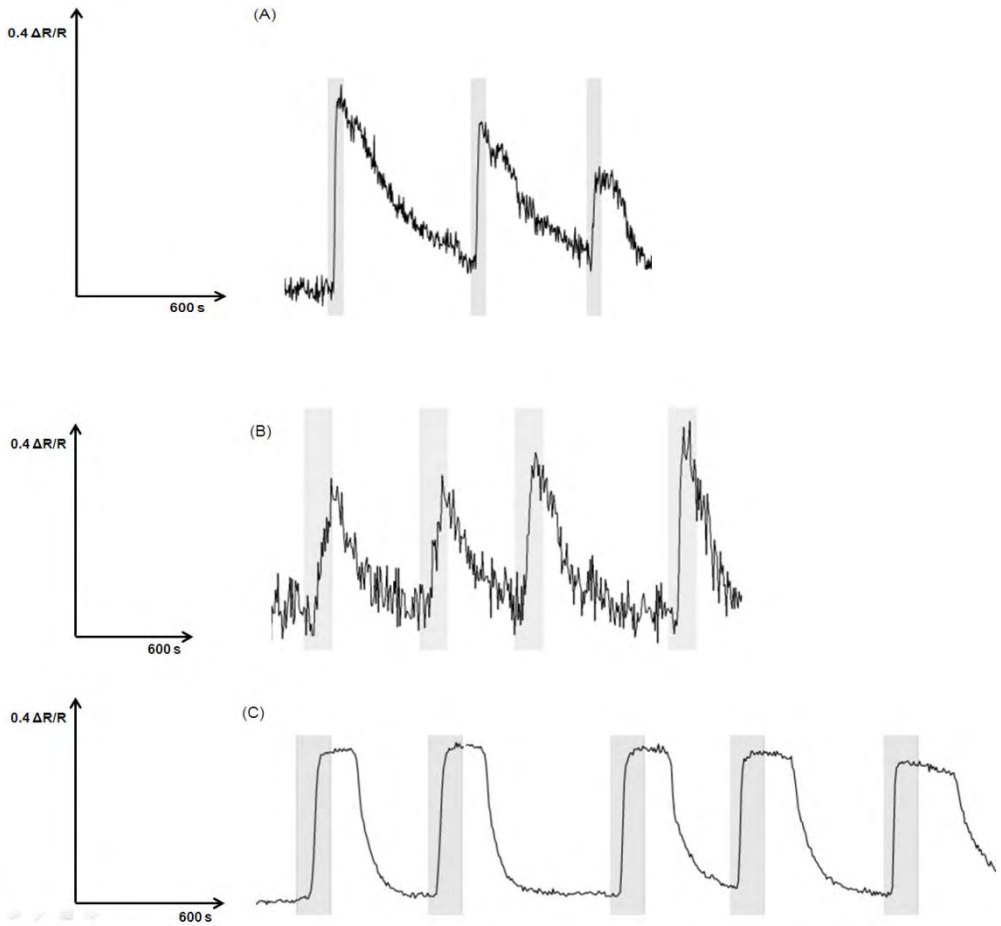

Figure 3.10. Dose-response experiments in aortic VSMCs (sensor: cGi500) applying ANP (A), CNP (B) and DEA/NO (C). The performed number of experiments is: (A) 1, (B) 3 and (C)

2; the number of VSMCs that are represented by this behavior of curves are: (A) 3, (B) 7 and (C) 18. The concentrations for each cGMP-modulating agent are the following: ANP: 85, 170, 210 nM, CNP: 16, 33, 50, 75 nM and DEA/NO: 33, 50, 80, 100, 200 nM. The grey rectangles indicate the respective drug application.

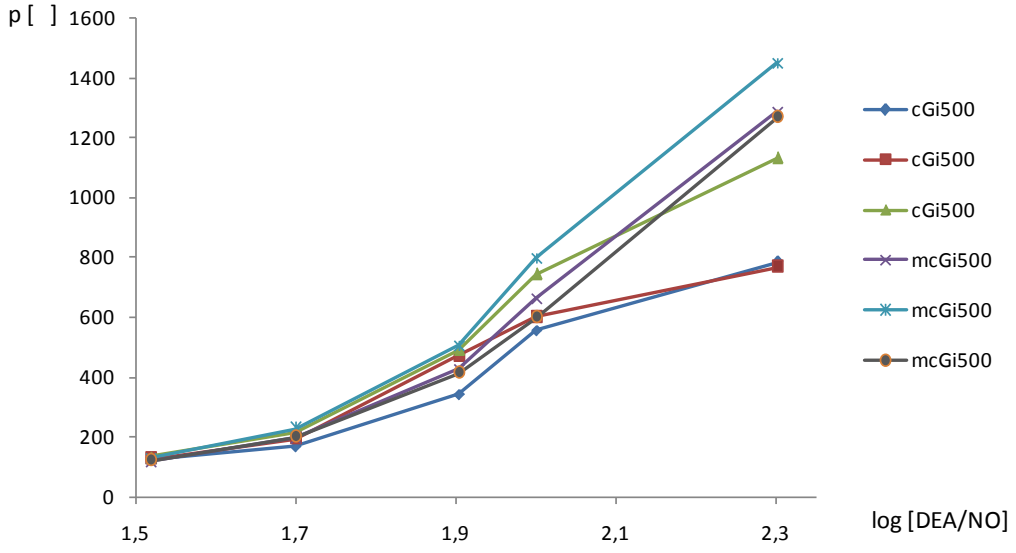

Figure 3.11. Graph depicting elevating p-values (*y* axis) in a representative DEA/NO dose-response experiment. The illustrated curves are associated with responses deriving from 6 representative VSMCs (3 for each of both cGi-type FRET sensors). The DEA/NO concentrations were calculated in the logarithm of 10 and are the following: 33, 50, 80, 100, 200 nM.

The aortic VSMCs as mentioned above, do not behave equally and most importantly it seems that there is a division into distinguished categories in the examined cell type. These “subpopulations” consist of three kinds at least: The aortic VSMCs which respond to CNP but much less intense to ANP and *vice versa* (example, figure 3.12, A), VSMCs which barely respond to CNP but they do respond after DEA/NO application (figure 3.12, B) and last but not least, VSMCs which respond to CNP but they cannot receive the cGMP-elevating stimulus after addition of DEA/NO (figure 3.12, C)

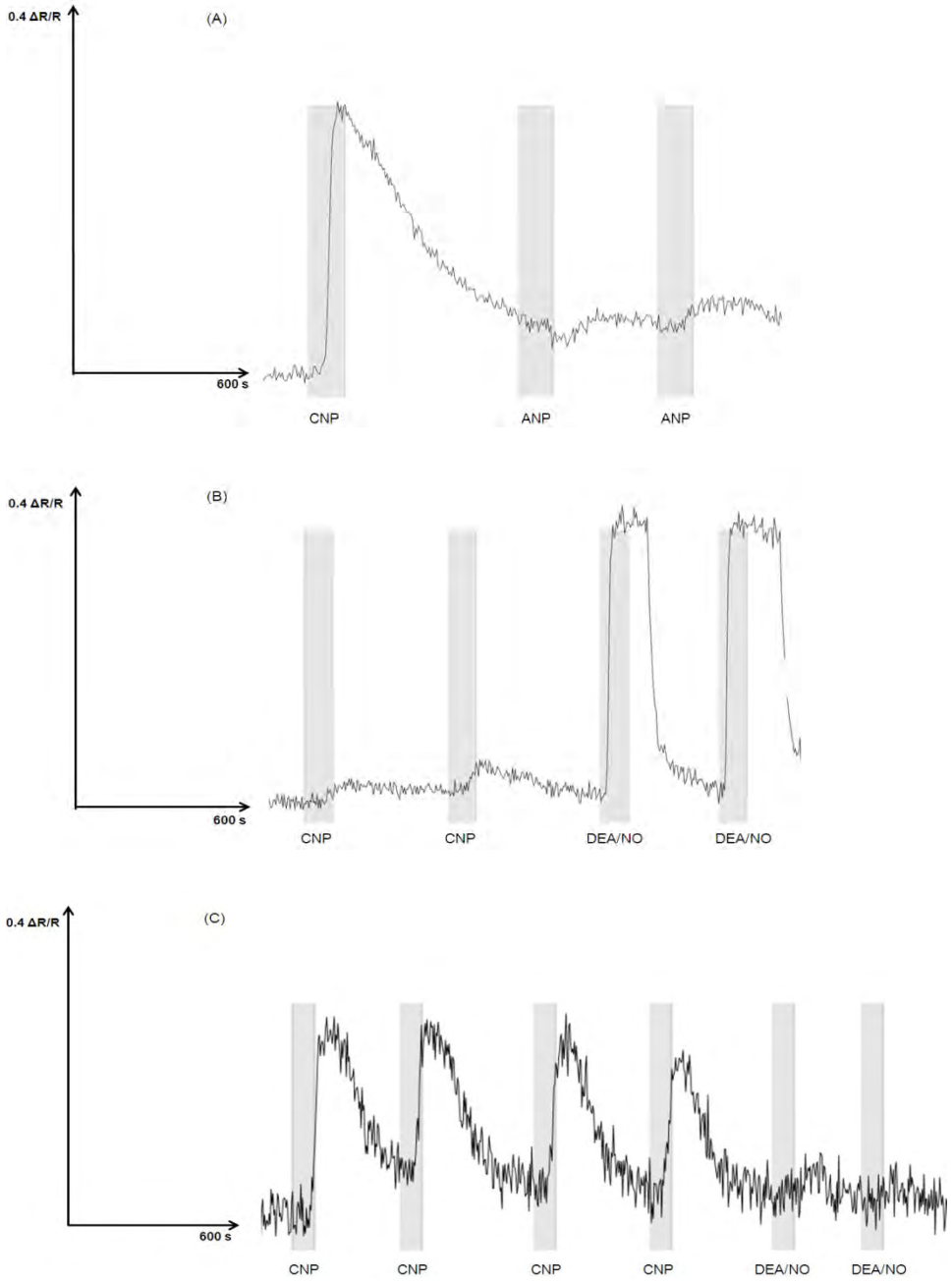

Figure 3.12. Differential FRET cGMP responses between aortic VSMCs, after serial applications of cGMP-modulating agents (ANP, CNP & DEA/NO) in rising concentrations. (A) Strong response to CNP and weak reaction to ANP; sensor: mcGi500. (B) Weak responses to CNP and strong reactions to DEA/NO; sensor cGi500. (C) Strong responses to CNP and weak-absent responses to DEA/NO; sensor: mcGi500. The grey rectangles indicate the respective drug application.

The results also demonstrated that in the case of CNP, there was a decrease in the time until response ("a" parameter) of aortic VSMCs between the first and second application (figure 3.13). The fact that cannot be excluded though, is that the two applications differed in concentration, with the latter being higher than the formal

one. For this reason, it was considered to perform again FRET measurements, applying this time the same concentration of CNP in order to investigate if it was really an effect of the concentration. From the new results it seems that there is such dependency, but a certain consensus cannot be drawn since there were cases in which VSMCs still reacted faster in the second application of the same concentration of CNP (figure 3.14).

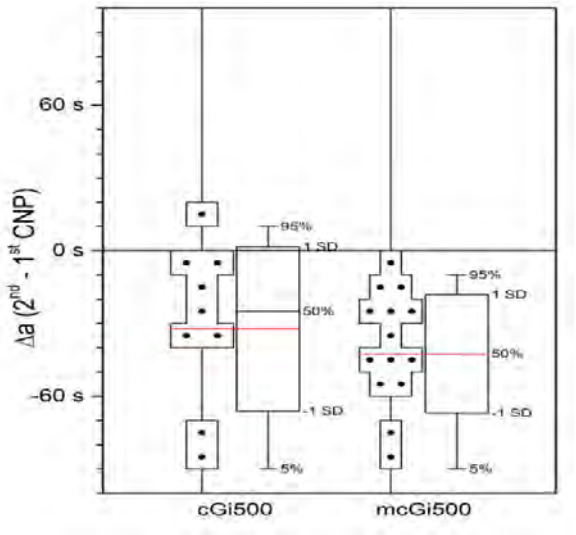

Figure 3.13. Difference in time (s) between the 2nd and 1st response (Δa) after CNP applications ([CNP]2nd>[CNP]1st), in aortic VSMCs expressing mcGi500 (14 cells) and cGi500 (9 cells). All VMSCs (apart from 1) demonstrate a faster CNP response (Δa<0). The box-plot refers to results deriving from 6 representative experiments.

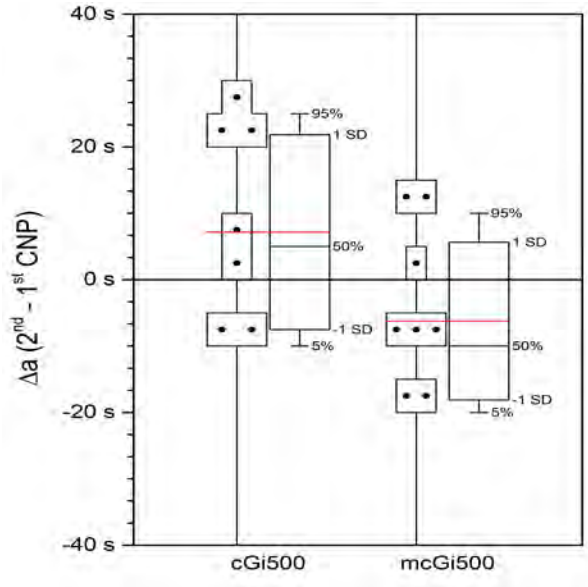

Figure 3.14. Difference in time (s) between the 2nd and 1st response (Δa) after applications of the same concentration of CNP in aortic VSMCs expressing the FRET cGMP biosensors mcGi500 (8 cells) and cGi500 (7 cells): VSMCs demonstrate a slower or unchanged (Δa≥0)

and a faster 2nd CNP response (Δa<0). The box-plot refers to representative examples of 3 relative experiments.

However what is clear from the latter experiments, is that there is a tendency for decrease in another important parameter: the height (h) of the curves, which represents the strength of each cGMP response within the VSMC. It was observed that this decrease through applications of the same concentration of CNP, occurred only conditionally: The aortic VSMCs which reacted relatively weakly to the first concentration of CNP and produced a FRET curve below or equal 0.1 ΔR/R, they could increase the peak height of their curves and therefore have a second stronger response to the same concentration of CNP (figure 3.15, A). In contrast, in VSMCs which firstly reacted over 0.1 ΔR/R (constituted the majority of cells), the height of their second FRET curve after application of the same dose of CNP was decreased in most cases or stayed in the same level (figure 3.15, B). Exceeding the second application of CNP while maintaining its concentration, the height of curves was ultimately reduced for every VSMC.

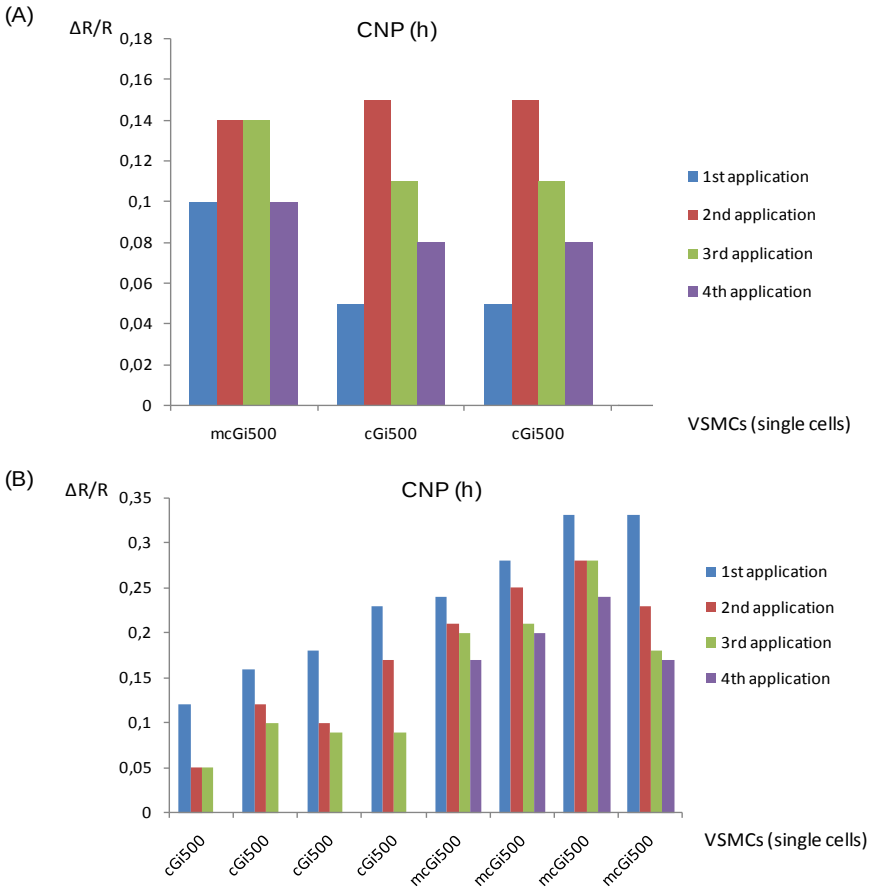

Figure 3.15. Differences in peak height (h, ΔR/R) of the responses between repetitive applications of the same concentration of CNP in aortic VSMCs: (A) 1st response of VSMCs,

below or equal of 0.1 ΔR/R, and (B) 1st response of VSMCs, over 0.1 ΔR/R. All the examined VSMCs demonstrate a decreasing tendency in the strength of their responses, after repetitive CNP applications with the same concentration. These graphs depict representative examples of 3 relative experiments.

3.4 Comparison of cGi500 and mcGi500 biosensors in aortic VSMCs

The FRET biosensors cGi500 and mcGi500 differ in localization as the cGi500 is located predominantly in the cytosol, while mcGi500 is located to the membrane. Hence, cells expressing these sensors may also differ in speed and intensity of FRET responses after receiving cGMP-elevating stimuli in the plasma membrane or in the cytosol via pGC and sGC receptors, respectively. In order to compare and contrast these biosensors, mixed cell cultures of primary VSMCs expressing the sensors were grown onto 13-mm coverslips of 24-well plates in normal cell culture medium (DMEM with 10% FBS). One day or two days prior FRET analysis, the medium was changed to be serum-free. The analyzed aortic VSMCs derived from four different batches of heterozygous transgenic mice (R26-CAG-mcGi500 and R26-CAG-cGi500).

Although isolated from different mice, mixed cell cultures provide the opportunity to analyze distinct VSMCs expressing either sensor, in the same field of view, at the same time, and under the same cell culture and imaging conditions. The amount of the examined aortic VSMCs for the comparison of the sensors, the days *in vitro,* and the experimental design in respect with the selected drug applications are depicted below (figure 3.16). The total number of examined VSMCs was 75 for cGi500 and 93 for mcGi500, while 10 VSMCs expressing mcGi500 that exhibited too much noise during FRET measurements, and 2 VSMCs that could not be identified regarding sensor expression, were excluded from the evaluation. Generally, mcGi500 exhibited more noise than cGi500 (figure 3.17).

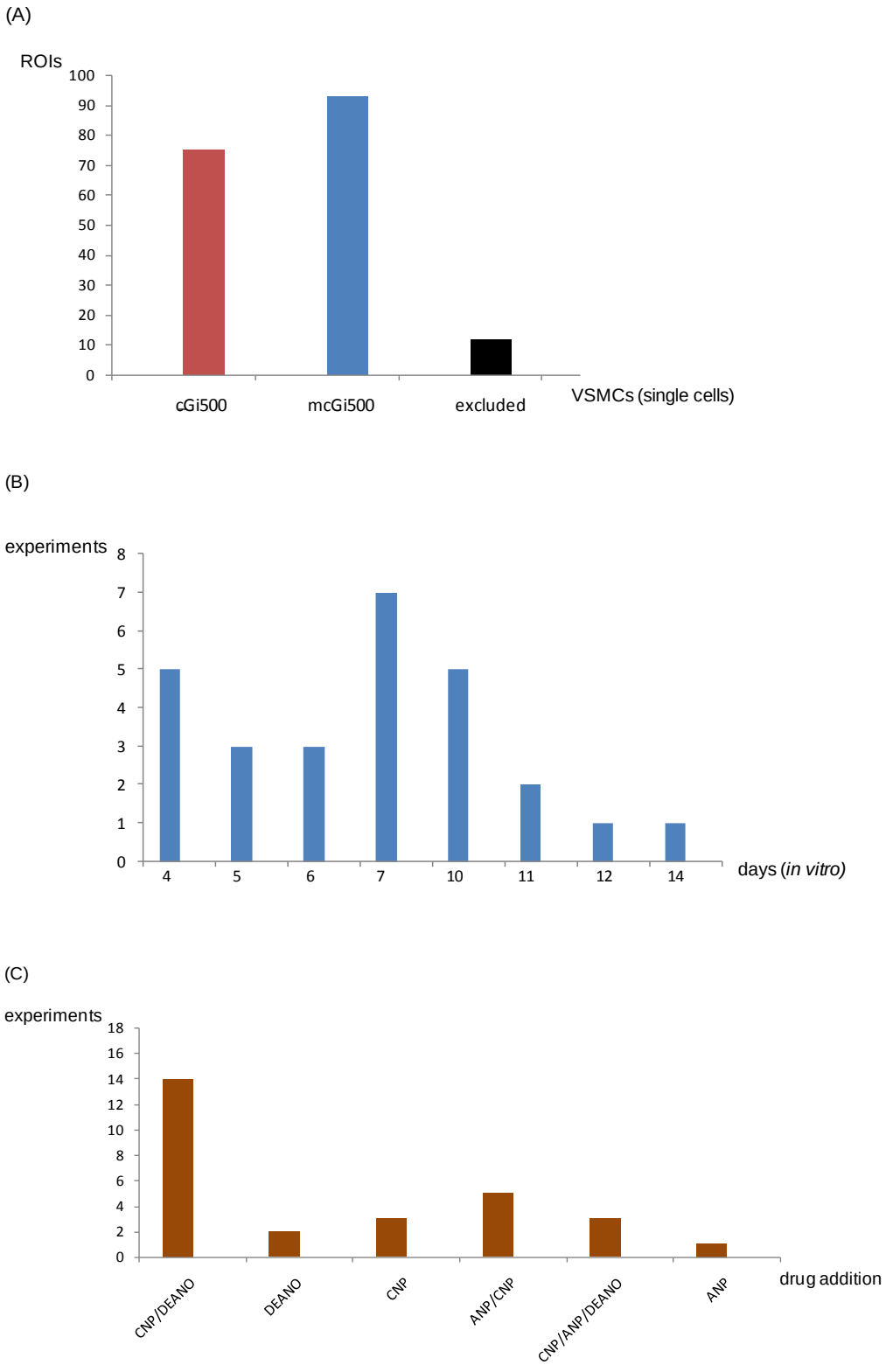

Figure 3.16. (A) Total number of examined VSMCs depicted in ROIs (B) days in cell culture (*in vitro*), (C) experimental design.

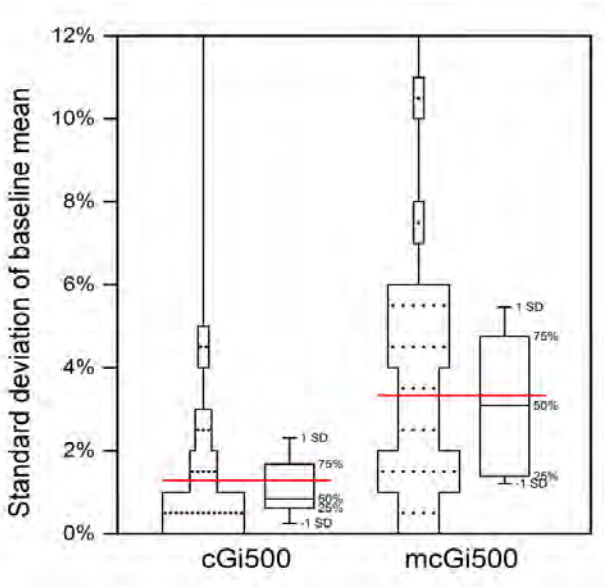

Figure 3.17. Box-plot depicting the standard deviation of baseline mean between cGi500- and mcGi500-expressing VSMCs (25 and 34 in number, respectively). Each dot represents a single VSMC and its respective value. The closer the value to 0%, the less noise is present.

CNP binds preferentially to the GC-B receptor which is located in the plasma membrane (Koller and Goeddel 1992). Therefore, experiments applying CNP as a cGMP-modulating agent would reveal if there are indeed differences between the VSMCs expressing mcGi500 and cGi500 regarding parameters which reflect for instance, the strength and speed of cGMP-FRET responses. DEA/NO was used as well, for this kind of comparison. The generated NO induces cGMP production through the sGC which is considered to be located in the cytosolic compartment (Mayer, Schmidt et al. 1989). Regarding the experimental design, CNP was either applied exclusively or before application of DEA/NO (figure 3.16, C).

3.4.1 CNP

For the comparison, many parameters regarding the curve of each response have been calculated, in order to detect the differences and elucidate partially into the cGMP-patterns after drug application. One crucial parameter is the peak height (h, ΔR/R) of the cGMP transient from the baseline, which indicates the strength of the cGMP response.

Regarding the CNP (50 nM) application, it was observed from a total of 12 experiments that 34% of VSMCs expressing cGi500 reacted weakly (“0-0.15 ΔR/R”), whereas the respective percentage for VSMCs expressing the mcGi500 biosensor was only 5%. In contrast, 81% of VSMCs expressing the membrane-bound biosensor

reacted relatively strongly, while only 49% of VSMCs expressing the cGi500 reacted similarly (figure 3.18, A).

As far as the CNP (100 nM) application is concerned, the percentage of VSMCs which reacted weakly was 3% for the mcGi500 and 31% for cGi500. Moreover, cells that reacted over 0.15% ΔR/R occurred more frequent for mcGi500 (90%) in comparison with the cGi500 biosensor (48%) (figure 3.18, B).

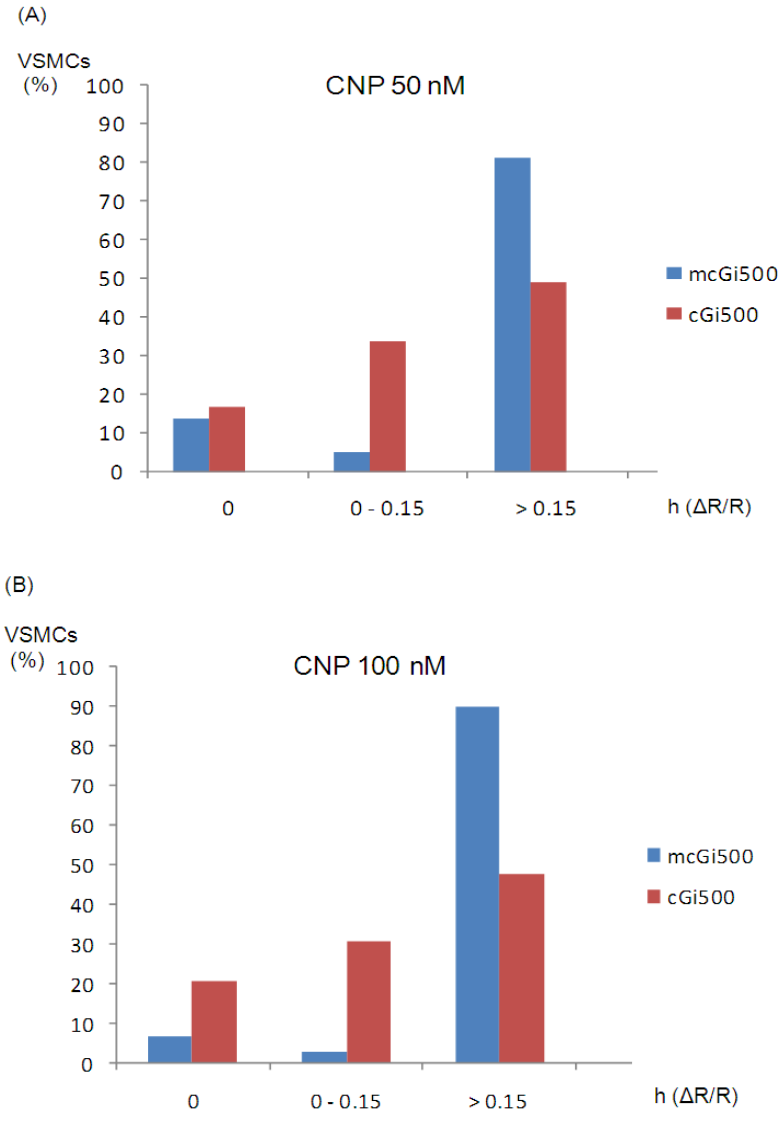

Figure 3.18. Comparative graphs depicting the strength of cGMP responses, as indicated by the height (h, ΔR/R) of the respective curves from VSMCs expressing either mcGi500 or cGi500 biosensor. “0 ΔR/R” indicates absent responses, “0-0.15 ΔR/R” weak and “>0.15 ΔR/R” mild-strong responses. (A) CNP 50 nM applications; 58 and 41 VSMCs out of 12 experiments were compared for mcGi500 and cGi500 biosensors, respectively. (B) CNP 100 nM applications; 31 and 29 VSMCs out of 10 experiments were compared for mcGi500 and cGi500 biosensors, respectively.

Apart from the “h” parameter, the rise (“p” parameter) of the curve is another important element to study possible differential responses among VSMCs expressing different sensors. It was observed in normalized p parameter values to DEA/NO (100 nM) that there are such dissimilarities, regarding the responses in various CNP concentrations (figure 3.19). The higher the p parameter, the more rapid and intense the cGMP increase is. According to these representative graphs, transgenic VSMCs which express the mcGi500 biosensor receive in general, more acutely the CNP-induced cGMP generating FRET-signal than those with the cGi500 biosensor.

(A)

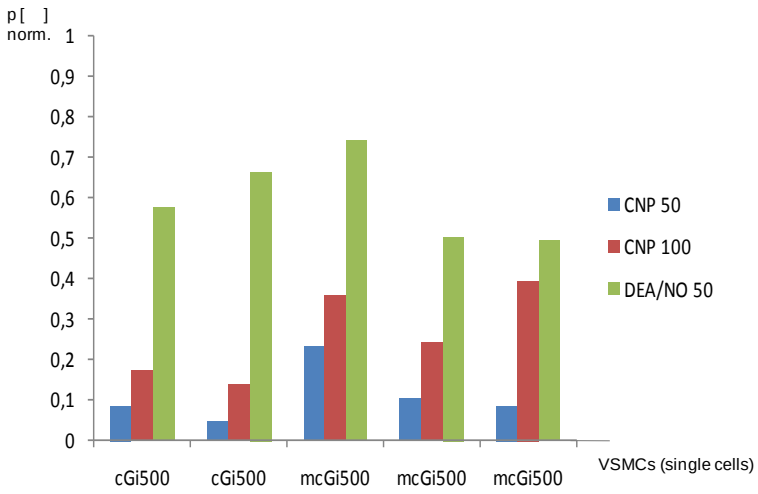

(B)

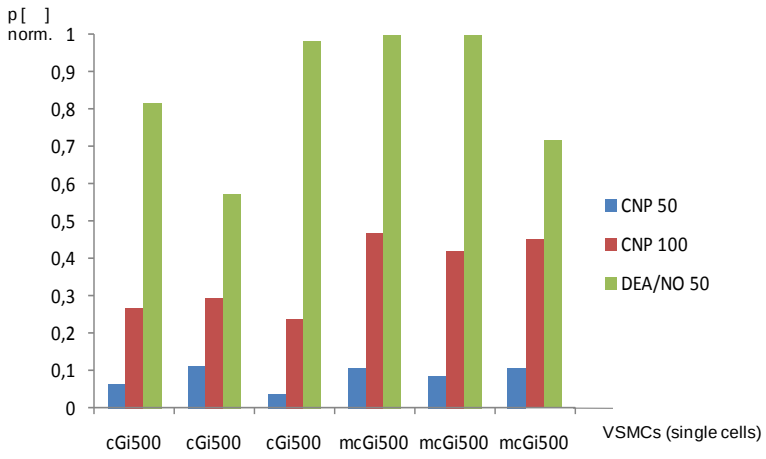

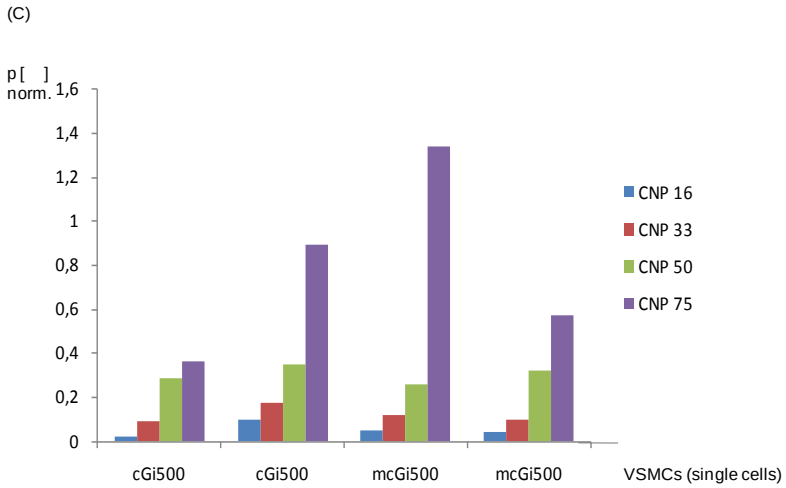

Figure 3.19. Representative examples out of 3 different experiments indicating the rise of cGMP transients ("p" parameter), after CNP applications, in VSMCs expressing mcGi500 and cGi500. Values of "p" parameter were normalized to DEA/NO (100 nM; p=1), and calculated as for: (A), (B) CNP (50, 100 nM), DEA/NO (50 nM), and (C) CNP (33, 50, 75 nM).

3.4.2 DEA/NO

As far as the DEA/NO applications are concerned, the parameters which were taken into consideration for the comparison of mcGi500 and cGi500 biosensors, were "a" and "c". The "a" parameter refers to the time of the drug application until a sufficient cGMP level is reached, which would indicate the time of response. As depicted in figure 3.20, the VSMCs expressing the two sensors differ only slightly in respect to this parameter. Furthermore, the two types of transgenic aortic VSMCs demonstrate also similarities after DEA/NO application, in relation with the "c" parameter which represents the time of application until the time in which the curve reaches its maximum (figure 3.21).

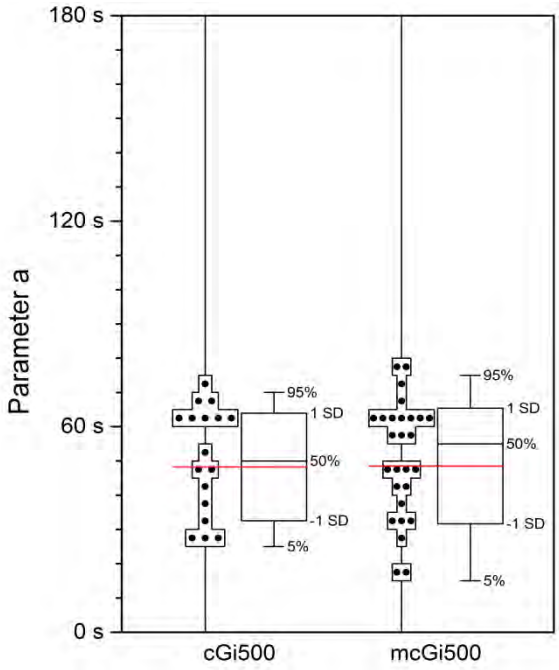

Figure 3.20. Box-plot associated with the time (s) of DEA/NO application until response ("a" parameter) of cGi500- and mcGi500-expressing VSMCs from the aorta. Each dot represents one single VSMC and its respective value of "a" parameter; 17 cGi500 and 27 mcGi500-expressing VSMCs were analyzed out of 5 experiments.

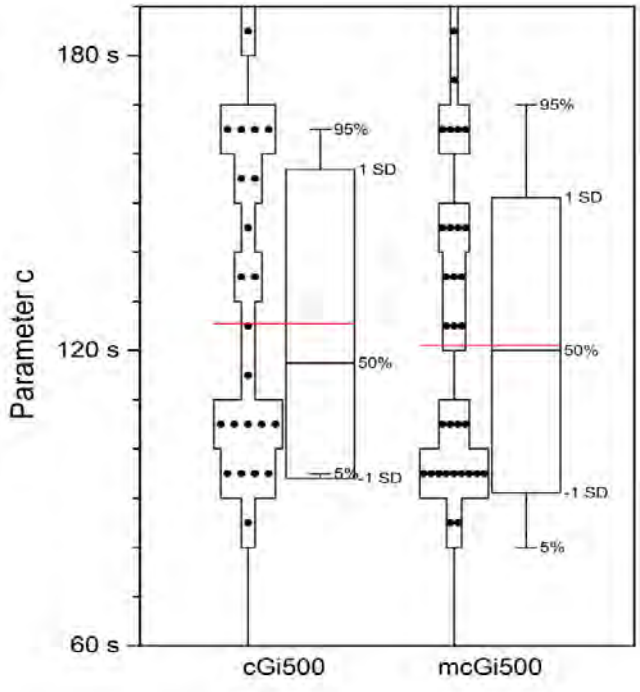

Figure 3.21. Box-plot regarding the time (s) of DEA/NO application until cGMP transient reaches its maximum ("c" parameter) between VSMCs from the aorta expressing cGi500 and mcGi500. Each dot represents a VSMC and its respective value of "c" parameter; 22 cGi500 and 31 mcGi500-expressing VSMCs were analyzed out of 6 experiments.

3.4.3 CNP versus DEA/NO

The cGMP signals that are exerted via two different pathways (CNP/GC-B and NO/sGC) were found to differ in the kinetics of the FRET curves. For instance in regard with the mcGi500 biosensor, the time of response after the first CNP application is higher than the respective time frame after the first DEA/NO addition (figure 3.22). Moreover, there are also differences in the rise of CNP- and DEA/NO-mediated cGMP transients (figure 3.19, A,B).

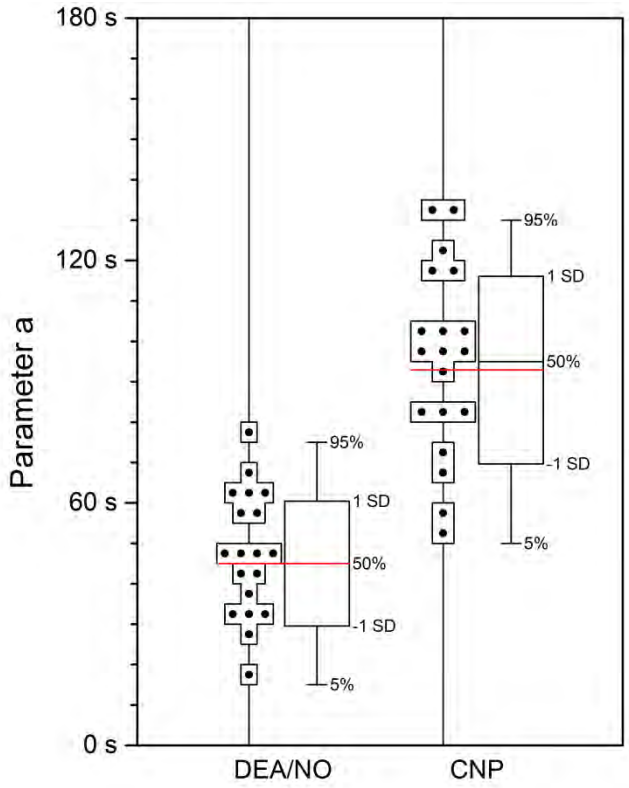

Figure 3.22. Differences in “a” parameter between first applications of CNP and DEANO in VSMCs expressing the membrane-bound mcGi500 biosensor. Each dot represents a single cell and its respective value of “a” parameter; 19 mcGi500-expressing VSMCs were analyzed for DEA/NO and 19 ones for CNP out of 4 relative experiments.

3.5 *In vitro* test for Cre-mediated induction of mcGi500 in smooth muscle cells (SMCs) from R26-CAG-mT/mcGi500 mice

R26-CAG-mT/mcGi500 transgenic mice carry a "*loxP*-silenced" mcGi500 transgene. These mice possess two *loxP* sites on either side of a membrane-targeted tdTomato (mT) cassette and show red fluorescence in all cell types examined. When bred to mice expressing Cre recombinase, the resulting offspring have the mT cassette deleted in Cre-expressing tissue(s) and one *loxP* site is now left, allowing expression of mcGi500 membrane-bound biosensor only in tissues/cell types of interest.

In this study, vascular, bladder, and colon smooth muscle cells (VSMCs, BSMCs, and CSMCs, respectively) were isolated from R26-CAG-mT/mcGi500 transgenic mice. It was tested whether Cre could induce the expression of mcGi500 *in vitro*. Furthermore, it was also tested whether the cGMP levels of those recombined cells could be monitored in real-time in FRET microscopy. The figure illustrated below prove that Cre-mediated excision is indeed achievable *in vitro* via protein transduction with HTNC: recombined cells expressing the mcGi500 FRET biosensor appear in color "green" (figure 3.23).

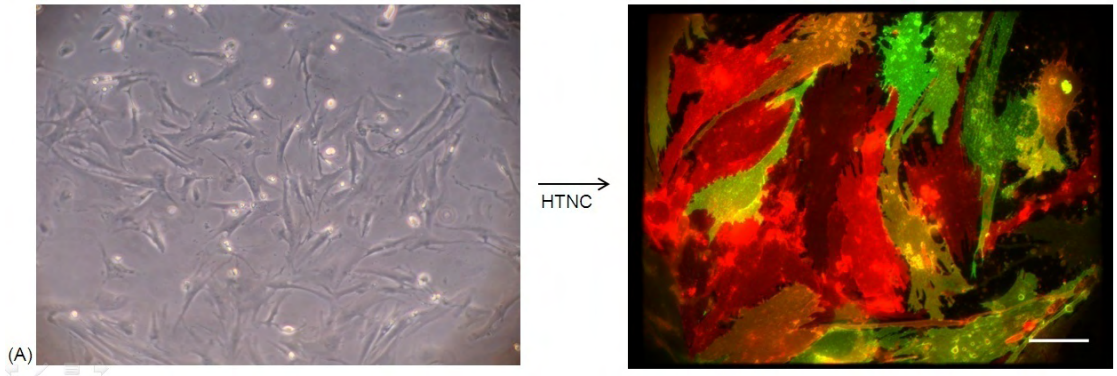

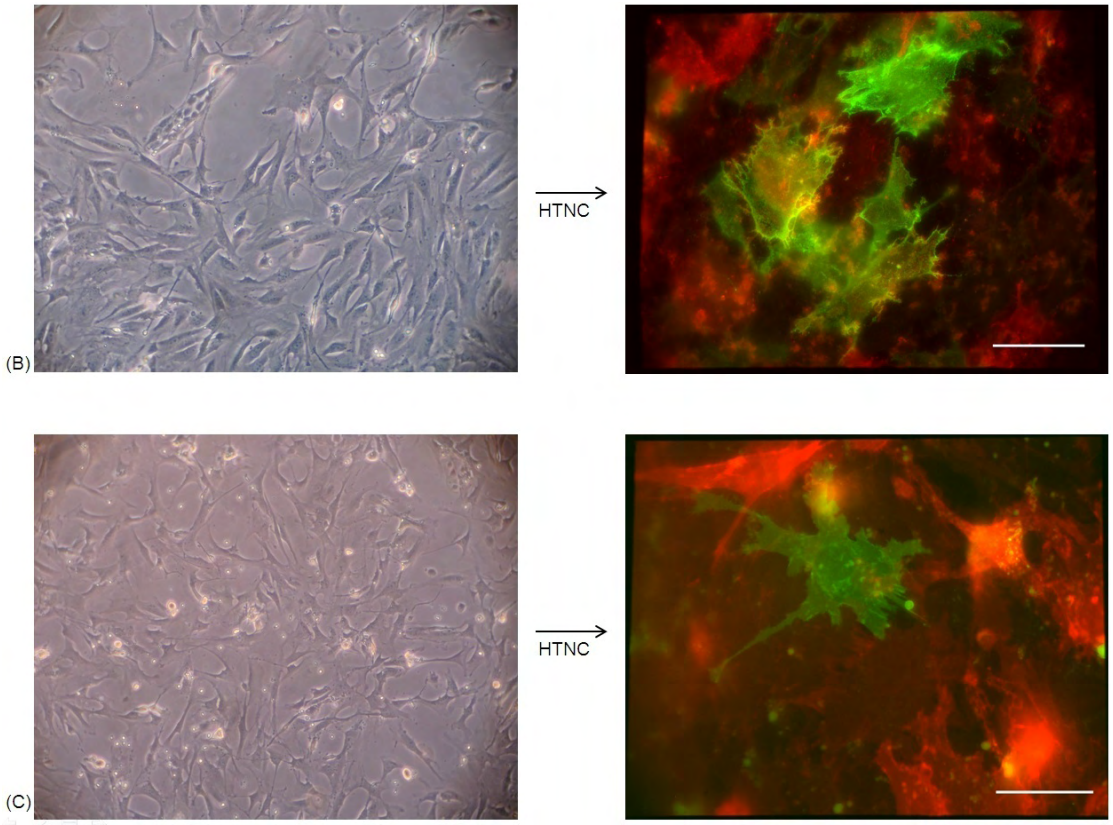

Figure 3.23. HTNC protein transduction in primary VSMCs from the aorta (A), BSMCs (B) and CSMCs (C) isolated from R26-CAG-mT/mcGi500 mice. The pictures on the left were obtained in 20x magnification, right before protein transduction, the 4th day after tissue isolation. The pictures on the right were obtained in 40x (A) and 64x (B, C) magnifications via epifluorescence microscopy (YFP and CFP channels), the day after protein transduction. Recombined SMCs are shown in green color, while non-recombined SMC appear in red. Note that the recombined VSMCs which appear in orange color, have not occurred by green and red cell overlay. Most probably they express mcGi500, but in the protein level, the expression of the “green” mcGi500 is low enough to prevail over the “red” mT. Scale bars: 35 μm.

Additionally, two days after protein transduction, FRET measurements were performed for each cell type expressing mcGi500. Aortic VSMCs were successfully monitored in respect to cGMP production, after stimulation with elevating concentrations of CNP and DEA/NO (figure 3.24). On the other hand, there were poor results for CSMCs and BSMCs as they seemed to be quite sensitive to photobleaching or to the imaging procedure, after the stress they had underwent through protein transduction.

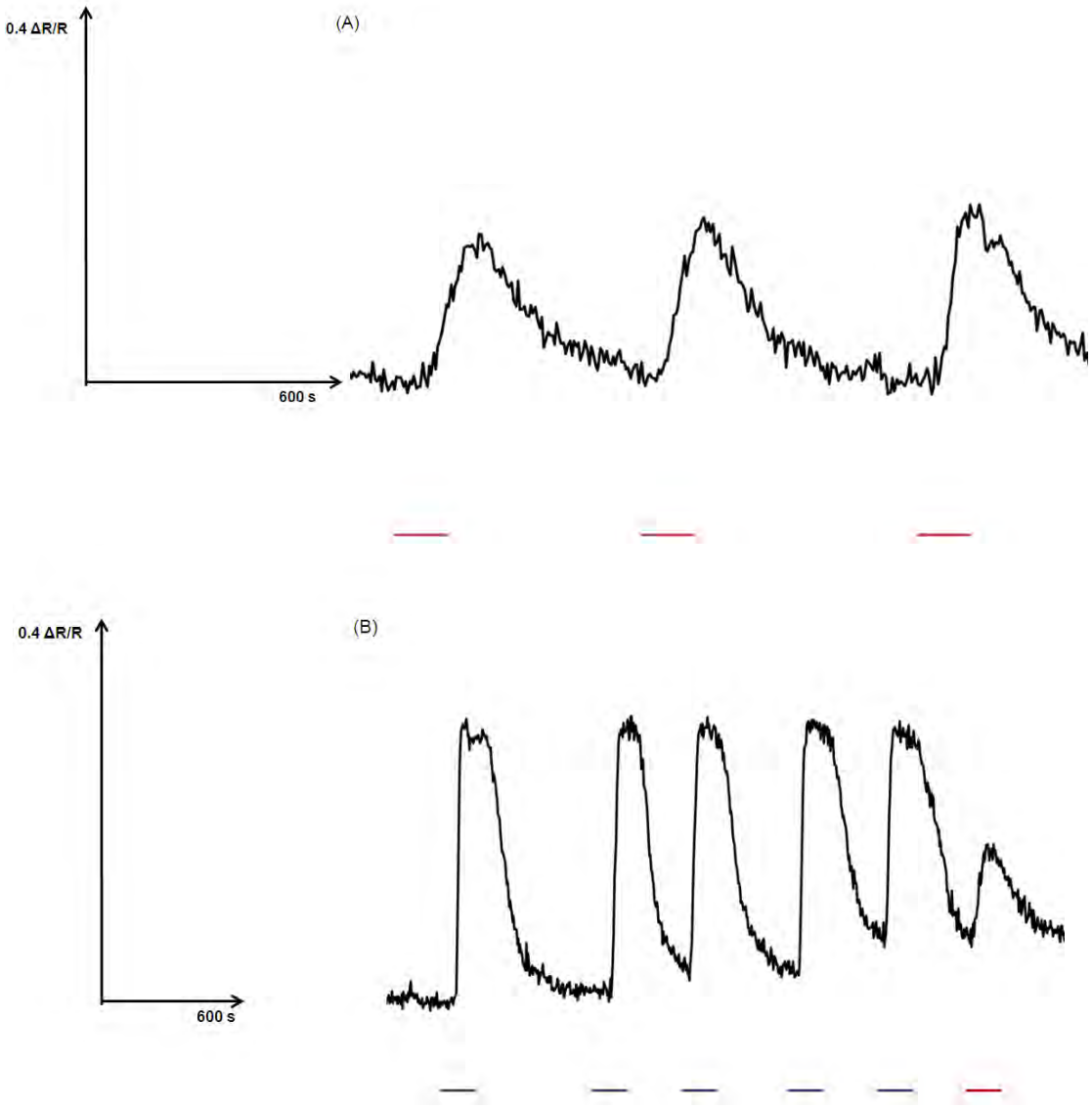

Figure 3.24. cGMP monitoring in dose-response experiments regarding: CNP (A) and DEA/NO (B) in HTNC-treated aortic VSMCs isolated from R26-CAG-mT/mcGi500 mice. The concentrations used for CNP dose-response experiment are: 50, 75 & 100 nM; for DEA/NO: 100, 150, 200, 250, 500 nM and lastly applied CNP 100 nM. Red bars represent CNP, while blue bars indicate DEA/NO applications.

4 Discussion

4.1 Compartmentalization of cGMP signals in VSMCs from the aorta

Recent studies have revealed that increases in cGMP levels triggered by NPs and NO donors lead to regulation of different cellular targets and procedures [(Zolle, Lawrie et al. 2000); (Rho, Perkins et al. 2002); (Zhang, Moalem et al. 2005)]. One model that explains the differential regulation of cellular processes such as growth, is the compartmentalization of cGMP-based cellular signaling (Piggott, Hassell et al. 2006). Therefore, cGMP signals may be compartmentalized or localized to distinct regions of the cell.

In this study, CNP and DEA/NO were used for the comparison of murine VSMCs from the aorta expressing either the mcGi500 membrane-bound biosensor or the cGi500 biosensor which is localized in the cytosol. One major obstacle in detecting the differences among them, was the genetic diversity that was present between the VSMCs deriving from the aortae of mice with different genome. Apart from that, differences in the phenotype of VSMCs, as indicated by the expression of a-smooth muscle actin, must have also contributed to this obstacle. However, our approach of seeding, growing, and then analyzing cGi500- and mcGi500-expressing VSMCs together, was to reduce as much as possible, any differences caused by preparation and culture. An issue that caused difficulties in the evaluation process, was the baseline noise that was mainly present in VSMCs expressing the mcGi500 biosensor. This noise was most probably correlated with the difference in brightness between the two sensors. The baseline noise could not be avoided as there was a compromise between photo-bleaching and illumination time. Consequently, some cells that were too noisy had to be excluded from the evaluation. Anyhow, the number of evaluated VSMCs which expressed the mcGi500 sensor prevailed eventually over the number of cGi500-expressing cells.

Despite all the mentioned impediments, results from the current study show that there are differential responses in mcGi500- and cGi500-expressing VSMCs after application of CNP. In total, CNP exerted stronger cGMP-FRET signals in VSMCs expressing mcGi500 than those with cGi500, as measured by two different parameters and evaluation strategies (“h” and “p” for Excel and Origin, respectively). Furthermore, the aortic VSMCs which responded weakly to this stimulus were much less in number for mcGi500 than for cGi500. This fact implies that CNP induces

cGMP production in the membranic fraction, but the generated cGMP may also spread and thereafter be detected in other regions within the cytosol.

As far as the DEA/NO applications are concerned, only slight differences were observed between VSMCs expressing the membrane-bound mcGi500 and those expressing the cytosolic cGi500 biosensor. These results are consistent with the literature as there are researches which prove that sGC which is the only proven receptor of NO to date, may translocate in the membranic fraction in some types of cells [(Zabel, Kleinschnitz et al. 2002); (Tsai, Liu et al. 2012)]. However, different types of experiments should be done to verify that this phenomenon does occur in the aortic VSMCs as well. Another intriguing possibility is that sGCs can be present in the cytosolic fraction but also very close to the membrane, so that the generated cGMP would be detected equally and simultaneously by both biosensors.

4.2 Mechanisms of receptor regulation

What was also evident from our results, is that there are differences in the kinetics of the cGMP transients of VSMCs upon CNP versus DEA/NO application. To be specific, the time from drug application until detectable response (i.e. cGMP production to a level of ~50-100 nM; Thunemann, Fomin et. al 2013) was lower for DEA/NO in comparison with CNP for both biosensors. Moreover, there were differences in the “p” parameter of the respective FRET curves, with the values of DEA/NO being always higher than for CNP, for both cGi500- and mcGi500-expressing VSMCs. These results indicate that there must be different regulation and activation mechanisms for the sGC and GC-B receptors within VSMCs from the aorta. DEA/NO induces faster cGMP production than CNP does. One possible explanation for this difference is that time of activation of the catalytic domain after ligand binding may be less for the sGC/Fe^{2+}/NO than the GC-B/CNP complex. Moreover, it could be also that there is a different catalytic speed of cGMP generation, dependent upon the amount of the sGC and GC-B enzymes present in VSMCs.

Experiments in which CNP was applied several times using the same concentration, exhibited also some interesting results. It was observed that at the end of the repetitive CNP application series, there was a decrease in the monitored cGMP levels produced within the VSMC compared to initial application(s) with the maximal cGMP levels as shown by the “h” parameter (ΔR/R). This phenomenon is

most probably attributed to the model of homologous desensitization of the GC-B receptor (Potter and Garbers 1992). Considering this model and the obtained results, it seems that there is an initial limit above which a receptor can be desensitized (0.1 ΔR/R). This observation implies that there is not always complete reduction in the phosphate content of the GC-B receptor after first CNP binding, so that the receptor would be fully desensitized. In contrast, upon first weak cGMP response that was below or equal of 0.1 ΔR/R, the GC-B receptor seemed to be sensitized or at least capable of producing higher cGMP levels upon second application of the same concentration of CNP. On the other hand, when the first cGMP response exceeded the limit which was above or equal of 0.12 ΔR/R, then the following cGMP responses were always less intense, indicating receptor desensitization. The reason why this phenomenon occurs conditionally, is not clear and further experiments should be performed to determine if or/and how this mechanism occurs *in vivo*.

From dose-response experiments applying ANP or CNP, it was shown that there are dissimilarities in the responses in elevating concentrations of the activators of GC-A and GC-B, respectively. Specifically, even if the concentration used in second application of ANP was 2-fold higher than the first one, there was a decrease in the strength of the second response compared to the formal one. Similarly, the next application which was close to 3-fold higher than the formal one, produced an even lower cGMP transient. This phenomenon was not present in CNP dose-response experiments. These results hint at a different rate of desensitization between the two kinds of pGCs in aortic VSMCs. However, facts that cannot be excluded are that the concentrations used in these experiments were not equal and plus, the number of experiments in which ANP was used, was considerably low due to availability issues. Therefore, more FRET measurements should be performed in order to verify the upper conclusion.

4.3 Differential cGMP responses induced by activators of pGC and sGC Receptors in VSMCs from the aorta

In this study, aortic VSMCs were found to behave unequally in cGMP-modulating factors such as CNP, ANP, and DEA/NO. For instance, a cell that was responsive to CNP did not receive such strong cGMP-elevating stimulus induced by ANP and *vice versa*. The same was observed between CNP and DEA/NO, even if reaction to CNP and not to DEA/NO happened most rarely. Hence, it was reasonable to consider that there is a categorization within aortic VSMCs, in respect to the differential responses

to NPs or/and DEA/NO. Below there are models which would try to provide a logical interpretation for this divisive phenomenon.

4.3.1 *In vivo*

One possibility that might occur *in vivo,* is that there are mechanisms of synergistic cooperation between the VSMCs in the aorta. It could be that this cooperation is evolutionarily developed in order to provide balance among the cGMP responses that are induced by different modulating agents. What is also possible is that these subpopulations of VSMCs exist, because they belong to distinct domains of the aorta which is the largest blood vessel in the body. For example, a VSMC derived from the aortic arch region may not behave similarly with another one from the subdominal aorta, in respect to cGMP signaling mediated by different factors such as ANP and CNP.

Another hypothesis is that aortic VSMCs are genetically pre-disposed to abnormal phenotype later in life, fact that might be the onset of aortic pathogenesis. For instance, if at any time a spontaneous, but harmful somatic mutation or other epigenetic event (e.g. methylation) occurs in the gene encoding for GC-B receptor of a VSMC which happens to be unresponsive to ANP already, then the consequent result would be that this impaired cell would not be able to receive a cGMP-elevating stimulus via the pGC pathway.

A pessimistic model to justify why these subpopulations occur within the same cell type, is that the integration of a gene encoding an artificial FRET biosensor in the genome (i.e. the ROSA26 locus) interferes with the native gene expression profile of mice. Even if this might occur to some extent, it is probably unlikely that the expression of the genes encoding for the pGC and sGC receptors is particularly affected. However, experiments need to confirm that there is not such interference.

4.3.2 *In vitro*

Taken into consideration that all the presented results stem from experiments in cell culture, one might believe that this categorization of aortic VSMCs may possibly not exist *in vivo*, as a change of the endogenous gene expression may happen *in vitro*. A loss of original gene expression might occur due to change of normal

microenvironment (*ex vivo* effect), cell culture conditions (media), and passaging. This view is highly acceptable, but it is also worthy to be mentioned that the results of this study derive from primary VSMC cultures mostly in passage 0, and cells were analyzed within two weeks after tissue isolation. Last but not least, it has been proposed that primary VSMCs cultured *in vitro,* undergo changes similar to those observed in neo-intimal VSMCs including decreased expression of specific genes and phenotypic switch [(Boerth, Dey et al. 1997); (Lincoln, Wu et al. 2006)]. Hence, it could also be the model of *in vitro* mimicking *in vivo* pathogenesis.

4.5 Outlook

In this study, it was revealed that aortic VSMCs exhibit a diversity in response to cGMP-elevating factors. This observation is in line with colleagues' results obtained with the same method (Lehners, Thunemann; unpublished). Moreover, it was shown that mcGi500 and cGi500 cGMP biosensors show a different subcellular localization. Dissimilarities were also exhibited regarding at least the responses upon CNP stimulation, while only slight differences were observed after DEA/NO application. What is more, the subcellular cGMP pools can be visualized but only partially, by utilizing the FRET principle in living cells expressing these sensors. All experiments mentioned above can be proved useful for our understanding of the spatiotemporal dynamics and the compartmentalization of cGMP signals inside VSMCs.

In the future, there are important experiments that should be conducted, apart from those suggested above. It seems to be that there is a high complexity in cGMP signaling via NPs and NO. Thus, the identification of the biochemical events that mediate the various effects of these molecules could provide novel targets for treatment of conditions including aortic pathogenesis, where intracellular cGMP compartmentalization may play an important role. The biosensors examined in the current study could be exploited in disease models to investigate possible effects in the normal compartmentalization of cGMP and its signaling pathways. A challenging concept for the study of subcellular cGMP pools would be to generate transgenic mice whose cells express biosensors in specific cellular microdomains such as in mitochondria, peroxisomes, and in the sarcoplasmic/endoplasmic reticulum. A variety of differentially localized FRET biosensors that could be used and detected at different wavelengths, at the same time would be invaluable for this kind of research. Even if this would be difficult to be achieved, mainly due to genetic manipulation constraints, it would provide the chance for researchers to penetrate into the

architecture of the cGMP signaling compartments in a plethora of cell types, in physiological and pathological conditions.

5. Acknowledgements

I would like to thank Prof. Dr. Robert Feil and Dr. Martin Thunemann for the given opportunity to join the laboratory and work under refined and inspireful conditions. I give much of my gratitude to my supervisor Dr. Thunemann for his kind assistance and useful advices that made the current work achievable and foremost pleasant. I thank also the people that co-worked in the laboratory and provided me prompt help and useful conversations: Barbara Birk, Jana Krauss, Michael Feyerabend, Moritz Lehners, Lai Wen, Raghavan Vallur and Sandeep Dhayade. I appreciate your time, patience and support. Special thanks to Lai Wen and Barbara Birk for contributing to the generation of the transgenic mice expressing the cGi500 and the mcGi500 sensors, respectively. Thanks to Dr. Michael Russwurm and his colleagues for the designing of FRET cGi-type biosensors. Moreover, I would like to thank also my coordinator from the department of Biochemistry & Biotechnology, University of Thessaly, Anna-Maria Psarra for her willingness, support and cooperation.

Most of all, I thank my parents, Ilias and Martha and my whole family for their encouragement, as well as for their mental and financial support which make my education possible to date.

I want also to show my appreciation to the staff of the ERASMUS program including Mrs. Hahne Simone, Mrs. Filomila Mougogianni and Dr. Frederic Brunner of ZMBP Tübingen, for making this movement a reality.

Last but not least, I like to express my gratitude to all my friends and especially to Athina Keramidiotou for the affection and support throughout the time.

6 References

Abbey-Hosch, S. E., et al. (2005). "Differential regulation of NPR-B/GC-B by protein kinase C and calcium." Biochem Pharmacol **70**(5): 686-694.

Alderton, W. K., et al. (2001). "Nitric oxide synthases: structure, function and inhibition." Biochem J **357**(3): 593-615.

Ashman, D. F., et al. (1963). "Isolation of adenosine 3', 5'-monophosphate and guanosine 3', 5'-monophosphate from rat urine." Biochem Biophys Res Commun **11**: 330-334.

Bellamy, T. C., et al. (2000). "Rapid desensitization of the nitric oxide receptor, soluble guanylyl cyclase, underlies diversity of cellular cGMP responses." Proc Natl Acad Sci U S A **97**(6): 2928-2933.

Bennett, B. D., et al. (1991). "Extracellular domain-IgG fusion proteins for three human natriuretic peptide receptors. Hormone pharmacology and application to solid phase screening of synthetic peptide antisera." J Biol Chem **266**(34): 23060-23067.

Biel, M. and S. Michalakis (2009). "Cyclic nucleotide-gated channels." Handb Exp Pharmacol(191): 111-136.

Boerth, N. J., et al. (1997). "Cyclic GMP-dependent protein kinase regulates vascular smooth muscle cell phenotype." J Vasc Res **34**(4): 245-259.

Bryan, P. M. and L. R. Potter (2002). "The atrial natriuretic peptide receptor (NPR-A/GC-A) is dephosphorylated by distinct microcystin-sensitive and magnesium-dependent protein phosphatases." J Biol Chem **277**(18): 16041-16047.

Casola, S. (2010). "Mouse models for miRNA expression: the ROSA26 locus." Methods Mol Biol **667**: 145-163.

Casteleyn, C., et al. (2010). "Validation of the murine aortic arch as a model to study human vascular diseases." J Anat **216**(5): 563-571.

Chabre, M., et al. (1993). "The G protein cascade of visual transduction: kinetics and regulation." Ciba Found Symp **176**: 112-120; discussion 121-114.

Chusho, H., et al. (2001). "Dwarfism and early death in mice lacking C-type natriuretic peptide." Proc Natl Acad Sci U S A **98**(7): 4016-4021.

Claxton NS, Laser Scanning Confocal Microscopy, non-published work

Couto, A., et al. (2013). "In vivo genetic dissection of O2-evoked cGMP dynamics in a Caenorhabditis elegans gas sensor." Proc Natl Acad Sci U S A **110**(35): E3301-3310.

Copeland, N. G., et al. (2001). "Recombineering: a powerful new tool for mouse functional genomics." Nat Rev Genet **2**(10): 769-779.

Court, D. L., et al. (2002). "Genetic engineering using homologous recombination." Annu Rev Genet **36**: 361-388.

De Duve, C., et al. (1955). "Tissue fractionation studies. Intracellular distribution patterns of enzymes in rat-liver tissue." Biochem J **60**(4): 604-617.

Derbyshire, E. R. and M. A. Marletta (2012). "Structure and regulation of soluble guanylate cyclase." Annu Rev Biochem **81**: 533-559.

Drewett, J. G., et al. (1995). "Natriuretic peptide receptor-B (guanylyl cyclase-B) mediates C-type natriuretic peptide relaxation of precontracted rat aorta." J Biol Chem **270**(9): 4668-4674.

Eiserich, J. P., et al. (1998). "Formation of nitric oxide-derived inflammatory oxidants by myeloperoxidase in neutrophils." Nature **391**(6665): 393-397.

Feil, R., et al. (2002). "Functional reconstitution of vascular smooth muscle cells with cGMP-dependent protein kinase I isoforms." Circ Res **90**(10): 1080-1086.

Feil, R. (2007). "Conditional somatic mutagenesis in the mouse using site-specific recombinases." Handb Exp Pharmacol (178): 3-28.

Feil, S., et al. (2009). "Inducible Cre mice." Methods Mol Biol **530**: 343-363.

Flora, D. R. and L. R. Potter (2010). "Prolonged atrial natriuretic peptide exposure stimulates guanylyl cyclase-a degradation." Endocrinology **151**(6): 2769-2776.

Forstermann, U., et al. (1991). "Isoforms of nitric oxide synthase. Characterization and purification from different cell types." Biochem Pharmacol **42**(10): 1849-1857.

Foster, D. C. and D. L. Garbers (1998). "Dual role for adenine nucleotides in the regulation of the atrial natriuretic peptide receptor, guanylyl cyclase-A." J Biol Chem **273**(26): 16311-16318.

Francis, S. H., et al. (2011). "Mammalian cyclic nucleotide phosphodiesterases: molecular mechanisms and physiological functions." Physiol Rev **91**(2): 651-690.

Fuller, F., et al. (1988). "Atrial natriuretic peptide clearance receptor. Complete sequence and functional expression of cDNA clones." J Biol Chem **263**(19): 9395-9401.

Furuya, M., et al. (1991). "C-type natriuretic peptide is a growth inhibitor of rat vascular smooth muscle cells." Biochem Biophys Res Commun **177**(3): 927-931.

Galkina, E. and K. Ley (2009). "Immune and inflammatory mechanisms of atherosclerosis " Annu Rev Immunol **27**: 165-197.

Gama Sosa, M. A., et al. (2010). "Animal transgenesis: an overview." Brain Struct Funct **214**(2-3): 91-109.

Gabbiani, G., et al. (1981). "Vascular smooth muscle cells differ from other smooth muscle cells: predominance of vimentin filaments and a specific alpha-type actin." Proc Natl Acad Sci U S A **78**(1): 298-302.

Hagiwara, H., et al. (1994). "Autocrine regulation of rat chondrocyte proliferation by natriuretic peptide C and its receptor, natriuretic peptide receptor-B." J Biol Chem **269**(14): 10729-10733.

Hamilton, D. L. and K. Abremski (1984). "Site-specific recombination by the bacteriophage P1 lox-Cre system. Cre-mediated synapsis of two lox sites." J Mol Biol **178**(2): 481-486.

Harder, A., et al. (1999). "Comparison of yeast cell protein solubilization procedures for two-dimensional electrophoresis." Electrophoresis **20**(4-5): 826-829.

Hassid, A., et al. (1994). "Nitric oxide selectively amplifies FGF-2-induced mitogenesis in primary rat aortic smooth muscle cells." Am J Physiol **267**(3 Pt 2): H1040-1048.

Inoue, K., et al. (2003). "Four functionally distinct C-type natriuretic peptides found in fish reveal evolutionary history of the natriuretic peptide system." Proc Natl Acad Sci U S A **100**(17): 10079-10084.

Jacobs, D. I., et al. (2001). "Sequential solubilization of proteins precipitated with trichloroacetic acid in acetone from cultured Catharanthus roseus cells yields 52% more spots after two-dimensional electrophoresis." Proteomics **1**(11): 1345-1350.

Joubert, S., et al. (2001). "Reduced activity of the NPR-A kinase triggers dephosphorylation and homologous desensitization of the receptor." Biochemistry **40**(37): 11096-11105.

Kanno, Y., et al. (2008). "Nitric oxide regulates vascular calcification by interfering with TGF- signalling." Cardiovasc Res **77**(1): 221-230.

Koller, K. J. and D. V. Goeddel (1992). "Molecular biology of the natriuretic peptides and their receptors." Circulation **86**(4): 1081-1088.

Koller, K. J., et al. (1993). "Proper glycosylation and phosphorylation of the type A natriuretic peptide receptor are required for hormone-stimulated guanylyl cyclase activity." J Biol Chem **268**(8): 5997-6003.

Koller, K. J., et al. (1991). "Selective activation of the B natriuretic peptide receptor by C-type natriuretic peptide (CNP)." Science **252**(5002): 120-123.

Kuhn, M. (2003). "Structure, regulation, and function of mammalian membrane guanylyl cyclase receptors, with a focus on guanylyl cyclase-A." Circ Res **93**(8): 700-709.

Labrecque, J., et al. (1999). "A disulfide-bridged mutant of natriuretic peptide receptor-A displays constitutive activity. Role of receptor dimerization in signal transduction." J Biol Chem **274**(14): 9752-9759.

Laemmli, U. K. (1970). "Cleavage of structural proteins during the assembly of the head of bacteriophage T4." Nature **227**(5259): 680-685.

Latt, S. A. and J. C. Wohlleb (1975). "Optical studies of the interaction of 33258 Hoechst with DNA, chromatin, and metaphase chromosomes." Chromosoma **52**(4): 297-316.

Lincoln, T. M., et al. (2006). "Regulation of vascular smooth muscle cell phenotype by cyclic GMP and cyclic GMP-dependent protein kinase." Front Biosci **11**: 356-367.

Lopez, M. J., et al. (1997). "The guanylyl cyclase-deficient mouse defines differential pathways of natriuretic peptide signaling." J Biol Chem **272**(37): 23064-23068.

Louis, S. F. and P. Zahradka (2010). "Vascular smooth muscle cell motility: From migration to invasion." Exp Clin Cardiol **15**(4): e75-85.

Lowry, O. H., et al. (1951). "Protein measurement with the Folin phenol reagent." J Biol Chem **193**(1): 265-275.

Lucas, K. A., et al. (2000). "Guanylyl cyclases and signaling by cyclic GMP." Pharmacol Rev **52**(3): 375-414.

Manenti et. al (1999). "Phosphorylation of the myristoylated protein kinase C substrate MARCKS by the cyclin E-cyclin-dependent kinase 2 complex in vitro." Biochem J **340** (3):775-82

Matsukawa, N., et al. (1999). "The natriuretic peptide clearance receptor locally modulates the physiological effects of the natriuretic peptide system." Proc Natl Acad Sci U S A **96**(13): 7403-7408.

Mayer, B., et al. (1989). "Biosynthesis of endothelium-derived relaxing factor: a cytosolic enzyme in porcine aortic endothelial cells Ca2+-dependently converts L-arginine into an activator of soluble guanylyl cyclase." Biochem Biophys Res Commun **164**(2): 678-685.

Metz, R. P., et al. (2012). "Vascular smooth muscle cells: isolation, culture, and characterization." Methods Mol Biol **843**: 169-176.

Miano, J. M. (2003). "Serum response factor: toggling between disparate programs of gene expression." J Mol Cell Cardiol **35**(6): 577-593.

Morris, M. C., et al. (2001). "A peptide carrier for the delivery of biologically active proteins into mammalian cells." Nat Biotechnol **19**(12): 1173-1176.

Nagase, M., et al. (1997). "Tissue distribution and localization of natriuretic peptide receptor subtypes in stroke-prone spontaneously hypertensive rats." J Hypertens **15**(11): 1235-1243.

Nandakumar, M. P., et al. (2006). "Proteomic analysis of extracellular proteins from Escherichia coli W3110." J Proteome Res **5**(5): 1155-1161.

Nausch, L. W., et al. (2008). "Differential patterning of cGMP in vascular smooth muscle cells revealed by single GFP-linked biosensors." Proc Natl Acad Sci U S A **105**(1): 365-370.

Nilles, K. M. and B. London (2007). "Knockin animal models of inherited arrhythmogenic diseases: what have we learned from them?" J Cardiovasc Electrophysiol **18**(10): 1117-1125.

Norris, R. P., et al. (2009). "Cyclic GMP from the surrounding somatic cells regulates cyclic AMP and meiosis in the mouse oocyte." Development **136**(11): 1869-1878.

Novak, A., et al. (2000). "Z/EG, a double reporter mouse line that expresses enhanced green fluorescent protein upon Cre-mediated excision." Genesis **28**(3-4): 147-155.

Peitz, M., et al. (2002). "Ability of the hydrophobic FGF and basic TAT peptides to promote cellular uptake of recombinant Cre recombinase: a tool for efficient genetic engineering of mammalian genomes." Proc Natl Acad Sci U S A **99**(7): 4489-4494.

Peterson, G. L. (1977). "A simplification of the protein assay method of Lowry et al. which is more generally applicable." Anal Biochem **83**(2): 346-356.

Piggott, L. A., et al. (2006). "Natriuretic peptides and nitric oxide stimulate cGMP synthesis in different cellular compartments." J Gen Physiol **128**(1): 3-14.

Placeres-Uray, F., et al. (2010). "Soluble guanylyl cyclase is reduced in airway smooth muscle cells from a murine model of allergic asthma." World Allergy Organ J **3**(12): 271-276.

Pollman, M. J., et al. (1996). "Vasoactive substances regulate vascular smooth muscle cell apoptosis. Countervailing influences of nitric oxide and angiotensin II." Circ Res **79**(4): 748-756.

Porter, J. G., et al. (1990). "Isolation and functional expression of the human atrial natriuretic peptide clearance receptor cDNA." Biochem Biophys Res Commun **171**(2): 796-803.

Potter, L. R. (1998). "Phosphorylation-dependent regulation of the guanylyl cyclase-linked natriuretic peptide receptor B: dephosphorylation is a mechanism of desensitization." Biochemistry **37**(8): 2422-2429.

Potter, L. R. (2005). "Domain analysis of human transmembrane guanylyl cyclase receptors: implications for regulation." Front Biosci **10**: 1205-1220.

Potter, L. R., et al. (2006). "Natriuretic peptides, their receptors, and cyclic guanosine monophosphate-dependent signaling functions." Endocr Rev **27**(1): 47-72.

Potter, L. R. and D. L. Garbers (1992). "Dephosphorylation of the guanylyl cyclase-A receptor causes desensitization." J Biol Chem **267**(21): 14531-14534.

Potter, L. R. and T. Hunter (1998). "Phosphorylation of the kinase homology domain is essential for activation of the A-type natriuretic peptide receptor." Mol Cell Biol **18**(4): 2164-2172.

Potter, L. R. and T. Hunter (2000). "Activation of protein kinase C stimulates the dephosphorylation of natriuretic peptide receptor-B at a single serine residue: a possible mechanism of heterologous desensitization." J Biol Chem **275**(40): 31099-31106.

Potthast, R., et al. (2004). "Calcium-dependent dephosphorylation mediates the hyperosmotic and lysophosphatidic acid-dependent inhibition of natriuretic peptide receptor-B/guanylyl cyclase-B." J Biol Chem **279**(47): 48513-48519.

Radi, R. (2004). "Nitric oxide, oxidants, and protein tyrosine nitration." Proc Natl Acad Sci U S A **101**(12): 4003-4008.

Rajalingam, D., et al. (2009). "Trichloroacetic acid-induced protein precipitation involves the reversible association of a stable partially structured intermediate." Protein Sci **18**(5): 980-993.

Ralat, L. A., et al. (2011). "Insulin-degrading enzyme modulates the natriuretic peptide-mediated signaling response." J Biol Chem **286**(6): 4670-4679.

Rensen, S. S., et al. (2007). "Regulation and characteristics of vascular smooth muscle cell phenotypic diversity." Neth Heart J **15**(3): 100-108.

Rho, E. H., et al. (2002). "Differential effects of soluble and particulate guanylyl cyclase on Ca(2+) sensitivity in airway smooth muscle." J Appl Physiol **92**(1): 257-263.

Rhodin JAG. (1979). "Architecture of the vessel wall." In: Berne RM, editor. Handbook of Physiology 1-31.

Ross, R. (1999). "Atherosclerosis--an inflammatory disease." N Engl J Med **340**(2): 115-126.

Rudijanto, A. (2007). "The role of vascular smooth muscle cells on the pathogenesis of atherosclerosis." Acta Med Indones **39**(2): 86-93.

Russwurm, M., et al. (2007). "Design of fluorescence resonance energy transfer (FRET)-based cGMP indicators: a systematic approach." Biochem J **407**(1): 69-77.

Saiki, R. K., et al. (1988). "Primer-directed enzymatic amplification of DNA with a thermostable DNA polymerase." Science **239**(4839): 487-491.

Sarkar, R., et al. (1996). "Nitric oxide reversibly inhibits the migration of cultured vascular smooth muscle cells." Circ Res **78**(2): 225-230.

Sassi, Y., et al. (2008). "Multidrug resistance-associated protein 4 regulates cAMP-dependent signaling pathways and controls human and rat SMC proliferation." J Clin Invest **118**(8): 2747-2757.

Sawa, T., et al. (2007). "Protein S-guanylation by the biological signal 8-nitroguanosine 3',5'-cyclic monophosphate." Nat Chem Biol **3**(11): 727-735.

Sayed, N., et al. (2007). "Desensitization of soluble guanylyl cyclase, the NO receptor, by S-nitrosylation." Proc Natl Acad Sci U S A **104**(30): 12312-12317.

Sayed, N., et al. (2008). "Nitroglycerin-induced S-nitrosylation and desensitization of soluble guanylyl cyclase contribute to nitrate tolerance." Circ Res **103**(6): 606-614.

Schopfer, F. J., et al. (2003). "NO-dependent protein nitration: a cell signaling event or an oxidative inflammatory response?" Trends Biochem Sci **28**(12): 646-654.

Schroter, J., et al. (2010). "Homologous desensitization of guanylyl cyclase A, the receptor for atrial natriuretic peptide, is associated with a complex phosphorylation pattern." FEBS J **277**(11): 2440-2453.

Schwarze, S. R., et al. (1999). "In vivo protein transduction: delivery of a biologically active protein into the mouse." Science **285**(5433): 1569-1572.

Silver FH, et al. (1989). "Mechanical properties of the aorta: a review." Crit Rev Biomed Eng **17**(4):323-358.

Sudoh, T., et al. (1990). "C-type natriuretic peptide (CNP): a new member of natriuretic peptide family identified in porcine brain." Biochem Biophys Res Commun **168**(2): 863-870.

Suga, S., et al. (1992). "Endothelial production of C-type natriuretic peptide and its marked augmentation by transforming growth factor-beta. Possible existence of "vascular natriuretic peptide system"." J Clin Invest **90**(3): 1145-1149.

Suo, J., et al. (2007). "Hemodynamic shear stresses in mouse aortas: implications for atherogenesis." Arterioscler Thromb Vasc Biol **27**(2): 346-351.

Surks, H. K. (2007). "cGMP-dependent protein kinase I and smooth muscle relaxation: a tale of two isoforms." Circ Res **101**(11): 1078-1080.

Thunemann, M., et al. (2013). "Visualization of cGMP with cGi biosensors." Methods Mol Biol **1020**: 89-120.

Thunemann, M., Wen, L. et al. (2013). "Transgenic mice for cGMP imaging." Circ Res **113**(4): 365-371.

Trachet, B., et al. (2009). "The influence of aortic dimensions on calculated wall shear stress in the mouse aortic arch." Comput Methods Biomech Biomed Engin **12**(5): 491-499.

Tsai, E. J., et al. (2012). "Pressure-overload-induced subcellular relocalization/oxidation of soluble guanylyl cyclase in the heart modulates enzyme stimulation." Circ Res **110**(2): 295-303.

Von der Leyen, H. E., et al. (1995). "Gene therapy inhibiting neointimal vascular lesion: in vivo transfer of endothelial cell nitric oxide synthase gene." Proc Natl Acad Sci U S A **92**(4): 1137-1141.

Weber, C. and H. Noels (2011). "Atherosclerosis: current pathogenesis and therapeutic options." Nat Med **17**(11): 1410-1422.

Yoder, A. R., et al. (2010). "Mass spectrometric identification of phosphorylation sites in guanylyl cyclase A and B." Biochemistry **49**(47): 10137-10145.

Zabel, U., et al. (2002). "Calcium-dependent membrane association sensitizes soluble guanylyl cyclase to nitric oxide." Nat Cell Biol **4**(4): 307-311.

Zaccolo, M. (2004). "Use of chimeric fluorescent proteins and fluorescence resonance energy transfer to monitor cellular responses." Circ Res **94**(7): 866-873.

Zhang, Q., et al. (2005). "Effects of natriuretic peptides on ventricular myocyte contraction and role of cyclic GMP signaling." Eur J Pharmacol **510**(3): 209-215.

Zolle, O., et al. (2000). "Activation of the particulate and not the soluble guanylate cyclase leads to the inhibition of Ca2+ extrusion through localized elevation of cGMP." J Biol Chem **275**(34): 25892-25899.